The representation of skin colour in medieval stained glasses: the role of manganese

Natan Capobianco[a], Myrtille O.J.Y. Hunault[b], Claudine Loisel[c,d], Barbara Trichereau[c,d], Fanny Bauchau[c,d,e], Nicolas Trcera[b], Laurence Galoisy[a], Georges Calas[a*]

[a]*Sorbonne Université, Muséum National d'Histoire Naturelle, UMR CNRS 7590, IRD, Institut de Minéralogie, de Physique des Matériaux et de Cosmochimie, IMPMC, 75005 Paris, France*

[b]*Synchrotron SOLEIL, L'Orme des Merisiers, BP 48 91192 Gif-sur-Yvette Cedex*

[c]*Laboratoire de Recherche des Monuments Historiques (LRMH), Ministère de la Culture, 77420 Champs-sur-Marne, France*

[d]*Centre de Recherche sur la Conservation (CRC), Muséum National d'Histoire Naturelle, CNRS, Ministère de la Culture, 75005 Paris, France*

[e]*Centre Interdisciplinaire de Conservation et de Restauration du Patrimoine (CICRP), 21 Rue Guibal, 13003 Marseille, France.*

* Corresponding author : Georges Calas , Sorbonne Université, IMPMC, BC 115, 4 place Jussieu 75005 Paris, France. georges.calas@sorbonne-universite.fr

Abstract

The present study concerns a corpus of 17 glass pieces representing character heads, originating from 11 major cathedrals and churches from North Western France and which constitute the masterpiece of stained glass windows. Skin complexion ranges from colourless to flesh-tone and purple. These glasses have been investigated using non-destructive and non-invasive techniques. Particle Induced X-ray Emission and Particle Induced Gamma Emission analyses at AGLAE show that these glass pieces show potassic plant ash glass compositions, typical to 12^{th} -15^{th} centuries. The compositional variability of the major glass components remains limited, similar to that found for single monuments, despite the diversity of geographic origins. The Mn and Ba concentrations follow a different trend in flesh-coloured or purple glasses and in colourless glasses, suggesting that the sources of Ba and Mn in these two kinds of glasses originated from different raw materials. Purple and flesh tone glasses contain more manganese than colourless glasses with an almost similar iron content. Synchrotron X-ray absorption near-edge structure spectroscopy (XANES) and portable UV-visible-NIR optical absorption spectroscopy indicate that glass colour varies with results from Fe^{2+}, Fe^{3+}, Mn^{2+} and Mn^{3+}. The thickness of the glasses, about 3mm, has been measured using ultrasound techniques. Its dispersion is similar in the various coloured glasses. This parameter mostly influences the colour saturation but not the hue. Obtaining flesh-coloured or purple glasses requires some control of the oxidation state of manganese during glass making. Divalent manganese is largely prevalent and the colour change from flesh-tone to purple hues is driven by small variations in the Mn^{3+} content. As these variations are not related to the Fe/Mn ratio, the resulting glass colour is difficult to predict on the only basis of glass composition. Due to the low kinetics for obtaining a redox equilibrium state between furnace atmosphere and the silicate melt, using Mn^{4+}- and Mn^{3+}-oxide minerals made it possible to favour oxidized melts, provided the glasses be taken out of the oven before redox equilibrium be reached: the shorter the melting time, the more oxidized will be resulting glass. This shows that medieval glassmakers were able to overcome the challenge of making glasses under highly oxidizing conditions to retaining enough oxidized manganese to favour flesh-tone and purple colours in wood-fuelled furnaces.

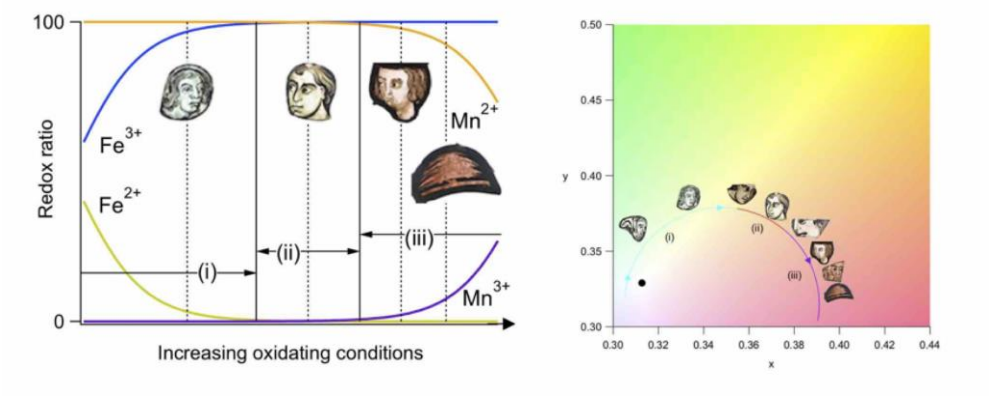

Graphical abstract. Left: Schematic evolution of the redox of Fe and Mn as a function of the oxidizing nature of the environment. Right: schematic trajectory followed by the colour of the glass in a CIE xy representation. The black dot corresponds to the white point for the D65 illuminant.

Keywords: Glass; Colorimetry; XANES; PIXE; Redox; Medieval glasses; Glass working.

1. Introduction

Stained glass windows play a central role in the medieval Gothic architecture and are invaluable witnesses of the evolution of the building technologies of this time (Rehren and Freestone, 2015). In addition to be an iconographic support, these translucent glass windows were bringing light and colour in the buildings (Simmons and Mysak, 2010 and 2012). On figurative panels, character heads are one of the most important glass pieces. Being painted using *grisaille* to represent the face features, these glass pieces demonstrate the highest skills of glass painters. The majority of medieval windows present six main colours: colourless, yellow, red, green, blue and purple. Purple plays a special role in the colour palette: dark purple is often used for clothing and light purple for skin complexion, heads and hands being among the brightest glasses. Their saturation remains low and their hues span from bluish or greenish to flesh-tone and pink (Capobianco et al., 2019).

Historical glasses are coloured by various elements, among which the most important are transition elements (copper, cobalt, manganese and iron) (Rehren and Freestone, 2015). By looking on the kaleidoscope that stained glass windows represent, it is possible to get information on medieval

glassmaking technologies and glass trade, in terms of raw materials and chemical composition, redox and fining conditions (Adlington et al., 2019; Henderson, 2013; Kunicki-Goldfinger et al., 2014; Hunault et al., 2016a and 2017a; Quartieri et al., 2005). Among colouring elements, manganese plays a special role, being added either to correct the greenish colour caused by ferrous iron impurities from raw materials, especially sand, or to colour the glass in purple. It is used as a decolouring agent since the Roman times (e.g. Bidegaray et al., 2019; Bingham and Jackson, 2008), a role also shown in Italian medieval glasses (Quartieri et al., 2005). In other cases, it is necessary to avoid the oxidation of the melt, as for obtaining reduced species: in red glasses, which require reducing elaboration conditions to allow the reduction of divalent copper to metallic nano-particles (Kunicki-Goldfinger et al., 2014). A recent study pointed out the absence of manganese, because of its role as a potential oxidant (Hunault et al., 2017a). The use of Mn as a colouring agent for purple and pink glasses has also been documented on old glass pieces, back to the Iron Age (Tite et al., 2008). Its presence in Roman glass is also frequent (Arletti et al., 2006; Bidegaray et al., 2019 and 2020).

Despite the important role of stained glass windows in medieval architecture (Herold et al., 2014), glassmaking at medieval times remains poorly understood. Few recipes about the fabrication of medieval purple glasses have been preserved. In early 12th century, Monk Theophilus (Hawthorne and Smith, 1979) only related what to do when a glass pot had come purple, but not how to intentionally make it so. Later, in the 15th century, Antonio of Pisa (Lautier and Sandron, 2008) reported that glassmakers used a ”stone from Aragon” to turn a naturally-greenish glass into colourless transparent glass, and that the use of larger amounts of this "stone" resulted first in flesh-coloured and then in purple glasses. This additive, also sometimes referred to as ”glassmakers’ soap”, contained an oxidized manganese mineral. Then, the question remains on how did the medieval glassmakers control, if they ever did, a reproducible final purple glass colour. In the case of purple glasses, the colour results from the presence of Mn^{3+} ions in the glass (Bamford, 1977; Bidegaray et al., 2019; Capobianco et al., 2019; Hunault et al., 2021). It is also used for depicting skin complexion in stained glass windows (e.g., Basso et al., 2009; Capobianco et al., 2021; Hunault et al., 2021; Palomar, 2018 and 2019). It is of interest that, in other glass-containing materials such as enamels (Biron and Verita, 2012) or tesserae (Verita and Santopadre, 2010; Schibille et al., 2018), a flesh tone colour has also been achieved by using thin layers coloured by gold nanoparticles deposited on a white enamel.

There is a lack of data on the way various parameters may influence the effect of manganese on the purple colour of medieval glasses, and about the relative influence of furnace temperature, length of firing time or oxidizing vs. reducing furnace atmosphere (Smith et al., 1987). Manganese concentration is also a major parameter. It may result from the use of manganese-bearing minerals, either as

impurities in the raw materials (e.g., Wedepohl and Simon, 2010) or intentionally introduced for colouring purpose. As raw materials (e.g. sand) also contain iron impurities, there is a mutual interaction between the redox equilibria of iron and manganese during melting, influencing the Mn^{3+} content of the glass and hence the final colour (Bidegaray et al., 2019 and 2020; Capobianco et al., 2019; Hunault et al., 2021). In medieval stained glass windows, dark purple glasses may contain on average about 50% more total manganese than colourless glasses, confirming the intentional addition of Mn-minerals (Gimeno et al., 2008; Hunault et al., 2021). Another route for favouring Mn^{3+} may result from melting and fining under oxidizing conditions and/or adjusting the melting temperature, though recent experimental evidence underlined the limited effect of the furnace's atmosphere to favour the presence of Mn^{3+} ions (Bidegaray et al., 2020). Recognizing these routes to obtain purple glasses may give precious indications about the technological mastering of glass making.

We report here the investigation of medieval glass pieces from 11 major French monuments, representing character heads. Each piece of glass was authenticated, allowing the reconstitution of their complex history. The skin complexion depicted on these glass pieces ranges from purple to flesh-tone and to colourless. These glass pieces provide an overview of the French glass production in the 12^{th}-13^{th} centuries, allowing relate glass colour to glass composition and fabrication conditions. Being removed from any panel, they could be easily analysed using non-invasive and non-destructive analytical methods. Optical absorption spectroscopy and synchrotron X-ray Absorption Near Edge Structure (XANES) provide a link between glass coloration and the speciation of transition elements (Calas et al., 2002). The present study aims at determining how medieval glassmakers managed the colours used to represent skin colour on the heads of important characters.

2. Materials

The 17 glass pieces selected for this study (Appendix A, Fig. A1 and Table A1) belong to a larger corpus of 62 stained glasses (see Supplementary Information A for further details). They have been substituted from their original panels during the 19th century and replaced by copies in the original windows. At the occasion of an auction selling, they were seized by French authorities. The glass pieces are in a very good state of conservation. An authentication was conducted on the basis of naked eye observation of the glass flatness, the style of the painting and by comparing with other medieval glass windows. Art historian's expertise allowed the identification of each piece of glass, including the precise origin of most of them. For certain pieces from the most famous monuments, it was even possible to identify the original bay and panel, as the substituted glass was a true copy of the original. These pieces originate from 11 major monuments located in North Western France, from late 12^{th} to

early 13th centuries. The selection of the glass pieces investigated has been done on several criteria: identification following art history criteria, diversity of the provenances, absence of major alteration of the glass surface. These unique pieces were entrusted to the Laboratoire de Recherche des Monuments Historiques (LRMH), as part of a study, while waiting a future exhibition project.

3. Analytical methods

3.1. Analytical methodology

The analysed zones were chosen preferentially on the internal surfaces, on areas devoid of paint. We conducted optical spectroscopy analyses on the entire corpus. Portable UV-visible-NIR absorption spectroscopy gave the concentration of the colouring species (Bidegaray et al., 2019 and 2020; Capobianco et al., 2019; Hunault et al., 2021; Meulebroeck et al., 2016). Ultrasound techniques have been used for thickness measurements. Chemical composition, including the concentration of transition elements, was determined by Ion Beam Analysis. It could only be carried out on a smaller part of the corpus, chosen so as to be representative of origins, colours and ages, and by favouring pieces from the most important historical monuments and the most documented history. X-ray absorption near-edge structure (XANES) spectroscopy was carried out on a subset of ten glass pieces whose chemical composition was known, providing the average speciation of iron (Ceglia et al., 2015; Vercamer et al., 2015) and manganese (Chalmin et al., 2009; Hunault et al., 2017a). The glass pieces 41 and 47-5 display, on the top of the head, a cap and a crown, respectively, that were analysed separately (Appendix, Fig. A1).

3.2. Chemical composition analyses

They were obtained by Particle Induced X-ray Emission and Particle Induced Gamma Emission (PIXE and PIGE, respectively) techniques at the AGLAE facility of the C2RMF in the Louvre (Paris, France) (Calligaro, 2008; Pichon et al., 2014; Van Wersch et al., 2013; Vilarigues and Da Silva, 2004; Vilarigues et al., 2019). PIXE and PIGE analyses were performed simultaneously on the glass pieces. PIXE analysis was performed using four fast counting SDD X-ray detectors: the first one is dedicated to the analysis of low Z elements ($10<Z<29$) and a helium flux is used to reduce the absorption of incident and remitted beams by air; the three other SDD detectors were dedicated to high Z elements ($Z>26$) and an aluminium filter is placed in front of each detector in order to absorb the low energy x-rays. One HPGe detector is used for the PIGE measurement. The 3 MeV incident proton beam, with an intensity of 3 to 4 nA, was focused to a 50 µm diameter on the target. The analysed area was 500 µm x

500 µm, which takes between 120 s and 300 s per analysis. The penetration depth ranges from 2 to 50 µm depending on the element analysed and the glass composition. For each glass sample, three measurements were performed at different positions to get an average composition of the analysed areas. The analyses were performed on the inner side of the glass pieces, after choosing a non-altered or less altered zone on the piece of glass and cleaning it with a water-ethanol solution. The spectra were extracted using TRAUPIXE, a software developed at AGLAE (Pichon et al., 2015), assuming that analysed zones be homogeneous and all elements present as oxides. The geochemical standard DR-N diorite and the reference Brill glasses, BrillA, BrillB, BrillC, BrillD, were used as reference materials to calibrate the PIGE data and control PIXE results. The compositions given in this paper result from the combination of PIXE data with the PIGE-derived sodium concentration.

3.3. Glass thickness

The thickness of each sample was determined using an Olympus ultrasound gauge 45MG-X-MT-E. An average value was obtained after five measurements on each piece of glass analysed by optical absorption spectroscopy (OAS) at the vicinity of the position of the zone analysed by OAS. Thickness homogeneity was further estimated by comparing with four other measurements at different positions on the sample.

3.4. Colorimetry and optical absorption spectroscopy

Optical absorption spectroscopy (OAS) has been performed in transmission mode with a specific mobile set-up described elsewhere (Capobianco et al., 2019; Hunault et al., 2016b). Spectra were measured between 4000 and 27000 cm^{-1}, with a lower sensitivity around 11000 cm^{-1}. Absorbance values have been extracted after subtracting a linear background absorption interpolated between the UV edge and near IR background. Colorimetric coordinates *xy* were computed from the measured spectra using the CIE (Commission Internationale de l'Eclairage) 1931 convention (see Supplementary Information B for further details). Assuming that Y represents mostly the lightness of a colour, the hue and saturation information is entirely contained in the x-y plane and can be summarized in chromaticity diagrams (Fig. 1a). By varying absorbance values by a 0.04 to 25 factor and calculating the corresponding *xy* coordinates, it is possible to calculate the variation of the colour of a glass with the same chromophore concentration and varying thickness or vice-versa. Such trajectories will be referred hereafter as *Beer-Lambert trend lines* (Capobianco et al., 2019).

3.5. X-ray absorption spectroscopy

XANES measurements at the Mn and Fe K-edge (6538 and 7112 eV, respectively) were performed at the LUCIA beamline of the SOLEIL Synchrotron facility (Saint-Aubin, France), operating in top-up mode at 2.75 GeV and 500 mA. A double crystal Si (311) monochromator was used, ensuring an energy resolution of 0.15 eV. Data were collected in fluorescence yield mode using a 4-element Si drift diode (SDD). The detectors were positioned at an angle of 90° to the incident beam. The beamline allows a micro-beam size of about 2*2 μm^2, which makes it possible to select glass surfaces that are devoid of excessive alteration and are not covered by grisaille. However, as the use of a microbeam causes photoreduction or photooxidation effects (e.g., Chalmin et al., 2009; Ferrand et al., 2015; Yamashita et al., 2004), the beam was defocused to cover a larger area (15x15 μm^2), reducing the exposure per unit area of the sample. The stability of the measurements suggests that possible photo-induced effects have a limited impact on the experimental redox values. The concentration of iron and manganese of the investigated glass pieces is above the detection limit, evaluated at about 100 ppm for XANES investigations. In addition, it is sufficiently low to neglect the self-absorption phenomena during fluorescence yield measurements. Spectra were normalized and processed using the ATHENA software (Ravel et al., 2005). Consistent spectra of different areas of the same glass were averaged to enhance the signal-over-noise ratio.

4. Results and discussion

4.1. The depiction of skin complexion varies from light blue to light purple

The colorimetric coordinates of the glasses analysed in PIXE/PIGE have been calculated in the Y*xy* and L*a*b* systems for the real sample thickness (Table C1, Appendix C). In Fig. 1, the CIE colour coordinates x and y of the investigated glass pieces are overlaid onto the CIE 1931 colour space, where any point in this xy diagram gives the chromaticity (hue and saturation) of the colour (Hunt and Pointer, 1991). Chromaticity spans over a broad colour range, from blue to orange and purple, with a relatively low saturation level, as compared to the other colours of medieval glasses (Capobianco et al., 2019; Hunault et al., 2021).

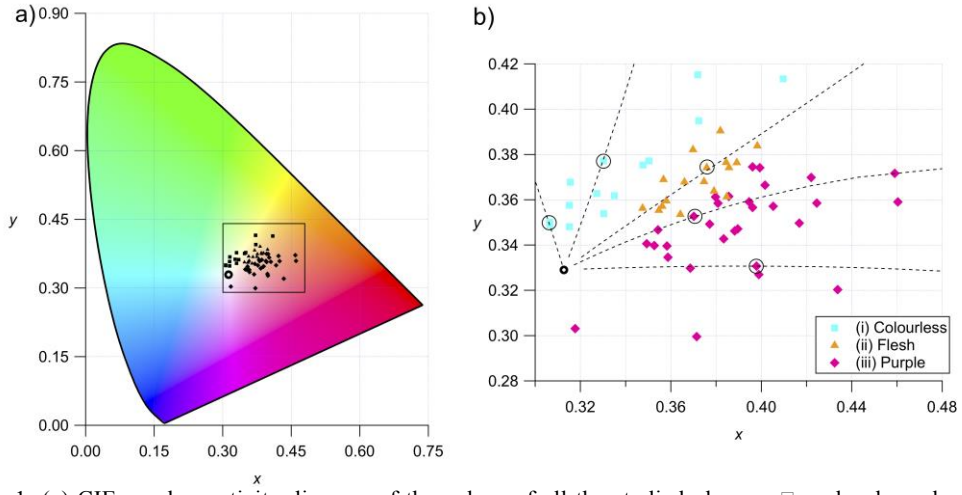

Fig. 1: (a) CIE xy chromaticity diagram of the colour of all the studied glasses. □: colourless glasses, △: flesh-coloured glasses, ◇: purple glasses. The white point bordered in black in the centre corresponds to the coordinates of the white colour. The region within the rectangle is zoomed in (b). Dashed lines in (b) show Beer-Lambert trend lines of selected glasses, describing how colour changes with glass thickness or the overall chromophore concentration, as derived from the experimental data (circled points).

Three main groups of colours will be used hereinafter: (i) blue to green hues and low saturation, referred to as colourless, (ii) yellow hues, referred to as flesh-tone, and (iii) orange to red and purple hues referred to as purple. Groups (ii) and (iii) are usually classified as purple by art historians. However, their distinction has proven useful here, as there is a chemical difference between them (see 4.4). Two main uses of purple glass are observed: character complexion using light purple or colourless glass and robes and dresses using more intense purple glass. While a clear frontier can be observed between the colorimetric coordinates of colourless and flesh-coloured glass pieces, Figure 1b shows that the distinction between flesh-coloured and purple glasses is less strict. The chromaticity of each group is in the same range as the ones observed in the contemporary glass windows of the Grande Rose of the cathedral of Reims, France (Capobianco et al., 2019). Glasses of the same origin and age (*e.g.* the two glass pieces from Chartres Cathedral) (Appendix A) can show different hues, which suggests that purple hue is neither specific of one production nor of one period.

4.2. Influence of glass thickness

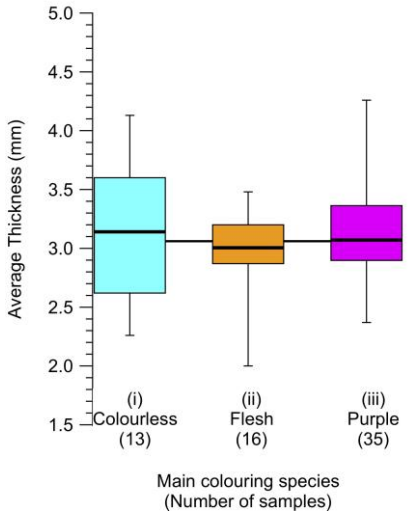

Fig. 2: Thickness statistics of the medieval glass pieces investigated.

As depicted in Fig. 2, the thickness statistics shows that these glass pieces only exhibit overall moderate thickness variations, ranging from 2 to 4.4 mm, with a median and mean value of 3.06 mm and 3.11 mm, respectively, and an overall standard deviation of 0.47 mm. Flesh-coloured glasses tend to be slightly thinner than the others with less thickness dispersion. There is no correlation between glass thickness and the dating (Supplementary Fig. S1). The relative standard deviation calculated on the five thickness measurements for each piece of glass does not noticeably change over the estimated fabrication date of the glass. The average thickness values are similar to those found in other gothic cathedrals (Reims, Sainte-Chapelle in Paris, Siena, Paderborn, Tarragona) (Basso et al., 2009; Capobianco et al., 2019; Garcia-Vallès et al., 2002; Hormes et al., 2013; Hunault et al., 2017) and for a set of medieval blue glasses (Hunault et al., 2016a).

The influence of thickness on glass colour can be modelled using Beer-Lambert trend lines (Fig. 1) and the normalization to a 3 mm thickness does not much change the colour perception (See Supplementary Fig. S2): it influences the saturation but not the hue, as the transmission window does not change with glass thickness. The thickness dependence of glass colour, recently evocated on Roman glass pieces (Bidegaray, 2020), only comes from a modification of the saturation level, defined by the intensity of the light transmitted by the absorption window. Spectroscopic

investigations are necessary do decipher between hue and saturation, in order to rationalize the visual observations made by a naked eye.

4.3. Chemical composition

The chemical composition of all the pieces of glass investigated by spectroscopy is reported on Table B1, Appendix B. Table 1 also reports the concentration and the relative standard deviation for 7 major glass components, by comparison with the values found for the stained glass windows of the York Minster, chosen as it is most likely imported from a single French supplier (Adlington et al., 2019) and the Nave of the Sainte Chapelle in Paris (Hunault et al., 2021) and the Abbey of Baume les Messieurs (Van Wersch et al., 2016), chosen as they were also analysed by PIXE-PIGE as in the present study.

These values indicate potash-lime silicate glasses, similar to the plant-ash medieval glasses elaborated during centuries in NW Europe (Adlington and Freestone, 2019; Schalm et al., 2007; Van Wersch et al., 2016; Wedepohl and Simon, 2010). The concentration of MgO and CaO characterizes the low lime-high magnesia group of plant-ash medieval glasses found in NW Europe (Kunicki-Goldfinger et al., 2014). The piece #47-28 from Dives sur Mer is an outlier, as it shows a Na_2O content of 2.3 wt.%, a value larger than in most glasses, where it remains near 1 wt.% and responsible for the large relative standard deviation observed for Na in this corpus. However, despite having the highest Cl content, the difference with the other glasses does not support that salt was used for glass making. On average, the concentrations found are similar to the values obtained on other French stained glass windows, including the early medieval glass pieces from Baume les Messieurs. Our data indicate low concentrations of most major components characteristic from the type of flux used to produce the glasses: Na_2O, MgO, K_2O, CaO and P_2O_5. By contrast, they show significantly higher silica values relative to the data on the York Minster.

Despite the pieces investigated are coming from 11 localities, the compositional variations remain limited and the relative standard deviation of this corpus remains similar to those found for single monuments. The compositional variability remains especially low for silica, lime and potash. The chemical compositions are also remarkably homogeneous in regard to the diversity observed during this period in Northern Europe (Adlington et al., 2019).

	Na_2O	MgO	Al_2O_3	SiO_2	P_2O_5	K_2O	CaO
This study							
Av. (wt%)	0.99	4.85	1.63	57.71	3.41	15.04	12.87
Rel. SD (%)	*49*	*17*	*17*	*4*	*23*	*10.3*	*8*
York Minster (Adlington and Freestone, 2019)							
Av. (wt%)	2.10	6.96	1.74	49.55	6.07	16.33	15.54
Rel. SD (%)	*25*	*8*	*17*	*6*	*18*	*14*	*9*
Nave, Sainte Chapelle (Hunault et al., 2021)							
Av. (wt%)	1.24	4.84	1.95	57.0	3.97	14.5	12.7
Rel. SD (%)	*57*	*19*	*11*	*4*	*14*	*13*	*13*
Early Medieval Baume les Messieurs (Van Wersch et al., 2016)							
Av. (wt%)	1.15	2.87	2.19	60.01	2.63	12.58	15.56
Rel. SD (%)	*23*	*26*	*30*	*4.25*	*22*	*16*	*13*

Table 1: Average values and relative standard deviation (compositional variability) of the chemical composition of the ancient glass pieces investigated in this study, obtained by PIXE-PIGE techniques, as the data on the nave of the Sainte Chapelle in Paris (Hunault et al., 2021) and those on the Abbey of Baume les Messieurs (Van Wersch et al., 2016). The data on from the York Minster glasses have been obtained by energy dispersive X-ray spectrometry (SEM-EDS) (Adlington and Freestone, 2019).

The ternary plot of SiO_2 versus Na_2O+K_2O versus $CaO+MgO$ (Supplementary Fig. S3) shows that the composition of the glass in terms of flux/silica ratio does not significantly vary. On the other hand, the ternary plot of K_2O+MgO versus Na_2O versus CaO shows that, despite being grouped in a limited zone of the plot, some glass compositions deviate from this group. These glass pieces correspond to the two pieces from Chartres cathedral (poorer in K_2O and MgO), to the two analyses of the yellow glass #47-28 (enriched in Na_2O, which is compatible with the fact that it comes from Normandy), and of two other glasses depleted in CaO (a purple glass of unknown origin and the white glass #42-5 of Saint-Germain-des-Prés).

Among the trace elements analysed, Ti and Zr are a useful indicator of the origin of sand raw materials (Aerts et al., 2003; Brems and Degryse, 2014; Lin et al., 2019). There is a correlation between Zr and Ti concentration in the glasses investigated (R=0.86), despite they were prepared at different times and different places (Fig. 3a). The Zr concentration is similar to that observed in continental Northern Europe (Aerts et al., 2003; Rehren and Brüggler, 2015), but Ti values are less dispersed. These elements are related to the presence of heavy minerals, zircon and rutile, in the sands used for glass making. As these minerals have a refractory character and Ti and Zr are non-volatile elements, the Zr/Ti ratio in the sand does not change

during glass melting, thus retaining the initial geochemical signature. This suggests that most glasses were produced with sands from similar geological sediments, using sources of production that were in use during decades.

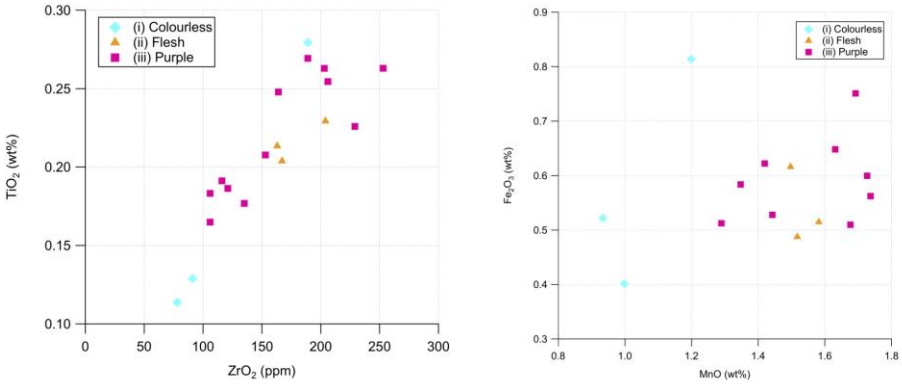

Fig. 3a, b. Biplots showing the composition of the colourless, flesh-coloured and purple glasses. (a, left): biplot of TiO_2 vs. ZrO_2. (b, right) Biplot of iron and manganese total contents as Fe_2O_3 and MnO oxides.

Manganese and iron are the two key transition elements responsible for the colour diversity from colourless to purple (Bidegaray et al., 2019 and 2020; Capobianco et al., 2019; Hunault et al., 2017a and 2021). Manganese concentration may reach relatively high values (average content: 1.5±0.5 wt.%). Iron concentration is significantly lower and close to the impurity level, 0.57±0.09 wt.%, a value close to the median average Fe_2O_3 concentration in medieval glass windows from North Western France, 0.61 wt.% (Adlington et al., 2019). All glasses have similar low contents in Fe_2O_3 (0.40-0.80 wt.%) regardless of their colour, above the impurity level concentration of about 0.5 wt.% Fe_2O_3 (Hunault et al., 2021). The MnO amount is higher in purple and flesh-coloured glasses (>1.2 wt.%) than in colourless glasses (<1.2 wt.%) (Fig. 3b), higher than the impurity level concentration of about 0.9 wt.% MnO found at Sainte Chapelle in Paris (Hunault et al., 2021). These values are similar to the concentration found in 13th century glass windows from NW France (Adlington et al., 2019). However, despite the Mn content is higher than that of other colouring ions, it does not allow discriminate purple and flesh-coloured glasses. As expected for French medieval glasses, the content of antimony oxide remains below the level of detection (LOD), showing that it was not used to decolour glasses.

4.4.Colouring role of Mn and Fe

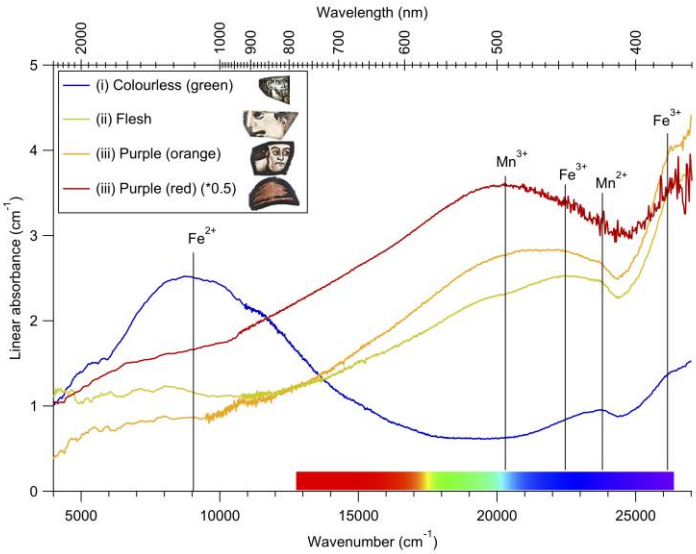

Fig. 4: Thickness normalized optical absorption spectra of four representative glasses. The Fe^{2+} absorption band is only visible in the colourless glasses, as Fe is mostly oxidized in the other glasses.

The spectra of colourless glasses are different from those of flesh-coloured and purple glasses. They show an intense and broad absorption band due to Fe^{2+}, centred in the near-IR around 9000 cm^{-1} and responsible for their light blue-green hue (Bamford, 1977). The weak and narrow bands at 22500, 24000 and 26300 cm^{-1} can be assigned to Mn^{2+} (Bingham and Parke, 1965; Möncke et al., 2013; Turner and Turner, 1970) and Fe^{3+} (Vercamer et al., 2015). They are responsible for the green shift of the hue.

The spectra of flesh-coloured glasses show the weak bands of Mn^{2+} (22500 cm^{-1}) and Fe^{3+} (22500, 24000 and 26300 cm^{-1}), superimposed to a rising background towards UV, due to the tail of an oxygen to Fe^{3+} charge transfer band as observed in oxidized glasses (Vercamer et al., 2015). The absorption band of Fe^{2+} is always absent in the spectra of these glasses. The shoulder at 20200 cm^{-1} (495 nm) corresponds to the broad absorption band of Mn^{3+}, in the middle of the visible range (Supplementary Fig. S4). Its relative intensity determines the colour of the glass. This Mn^{3+} absorption band dominates the spectra of purple glasses and hinders the observation of the weak Mn^{2+} and Fe^{3+} absorption bands. The Fe^{2+} broad absorption band is always absent, demonstrating a full oxidation of iron in these glasses. The Mn^{3+} absorption band absorbs in the green spectral domain,

while presenting two transmission windows, one in the near UV and the other in the near IR region: the resulting colour is intense reddish purple, due to light absorption over most of the visible spectrum.

4.5. Determination of iron and manganese redox states: Mn is mostly divalent and Fe mostly trivalent

The concentration of Mn^{3+} and Fe^{2+} can be determined by optical absorption spectroscopy (OAS), using molar extinction coefficient (ε) values from soda-lime glasses, $\varepsilon_{Fe^{2+}}$=27.5 L/mole/cm (Ceglia et al., 2015) and $\varepsilon_{Mn^{3+}}$ = 130 L/mole/cm (Capobianco, 2018), in the absence of data available for potash-lime glasses. The OAS data on colourless and flesh-coloured glasses show only a weak contribution of Mn^{3+}, with a Mn^{3+}/Mn_{total} ratio below 1%. The intensity of the Fe^{2+} absorption band shows that the Fe^{2+}/Fe_{total} ratio spans over a large interval from 57±8% for the greener glass to 22±3% for the yellower one. In flesh-coloured and purple glasses, the Mn^{3+}/Mn_{total} ratio spans from 0 to 4% (with a 20% relative error, excluding the uncertainty on the molar extinction coefficient value), the higher values corresponding to more purple hues. In these purple glasses, OAS data show no significant Fe^{2+} contribution.

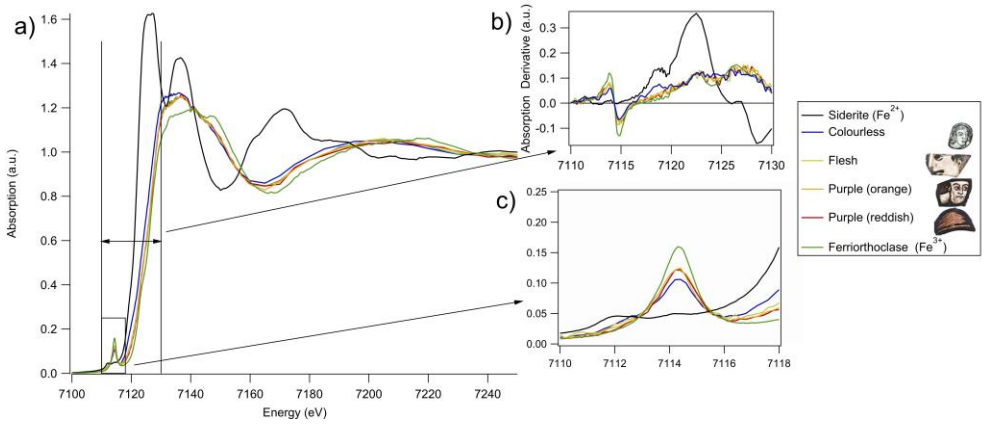

Fig. 5: a) Fe K-edge XANES spectra of four samples representative of the various hues and two crystalline references b) derivative and c) zoom on the pre-edge.

The absence of significant Fe^{2+} contribution in the OAS data of flesh-coloured and purple glasses, agrees with Fe K-edge XANES spectra (Fig. 5): they show a similar pre-edge feature, both in shape and relative intensity. The shape and position are close to the spectrum of the tetrahedral Fe^{3+} crystalline reference (ferri-orthoclase), as indicated by the derivative functions, but the intensity is reduced by about 35% relative to this reference, indicating the presence of reduced Fe that is not detected by OAS due to the large width of the absorption band. In colourless glasses, the intensity of the pre-edge is reduced by about 50% relative to ferri-orthoclase. In addition, the shape of the pre-edge peak on its low energy side indicates the presence of Fe^{2+}, as in the Fe^{2+} reference (siderite), which is consistent with a 50% proportion of Fe^{2+} as in other reduced historical glasses (Arletti et al., 2013).

The XANES spectra at Mn K-edge (Fig. 6) are nearly identical to each other and occur at the same position as in the tetrahedral Mn^{2+} reference, jacobsite. This shows that, in all glasses, Mn occurs mostly in the Mn^{2+} state. The low intensity comes from a difference in site symmetry (i.e. tetrahedral in jacobsite vs. 5- or 6-coordinated sites in glasses). Purple glasses show a slight shift of +0.2 eV in the energy position of the pre-edge (Fig. 6c), which indicates an Mn^{3+}/ Mn_{total} ratio of about 4%, a value higher than in other glasses (Chalmin et al., 2009).

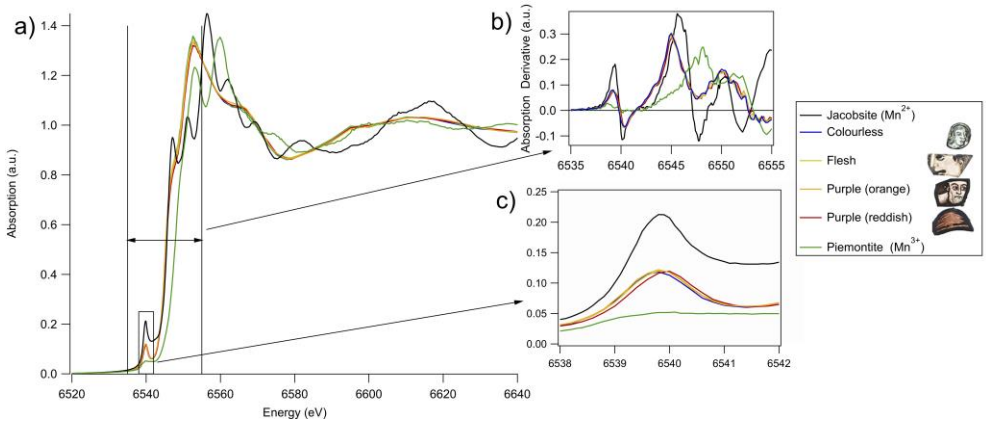

Fig. 6: a) Mn K-edge XANES spectra of four samples representative of the various hues at and two crystalline references b) derivative and c) zoom on the pre-edge.

Only a small fraction of manganese is present as Mn^{3+} despite it is responsible for the purple to flesh-tone colours. Even small variations have a drastic impact on this colour. The concentration of Mn^{3+} in the glass depends on the Mn_{total} content and on the Mn^{3+}/Mn_{total} ratio. The saturation of the purple colour is not related to the Mn_{total} concentration (size of the open markers on Fig. 7), but there is a correlation with the Mn^{3+}/Mn_{total} ratio evaluated from the spectroscopic data (grey scale in the open markers on Fig. 7) derived from spectroscopic data (Fig. 7). As these glasses show a similar Mn_{total} content, the variation of the manganese redox ratio is responsible for the change of hue.

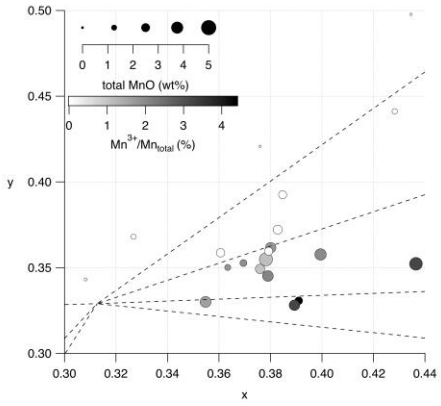

Fig. 7: CIE xy colour plot of the stained glasses, showing the relative influence of Mn^{3+} concentration (grey scale of the open markers) and total manganese content (open markers' size).

4.6. Control of the redox conditions: Influence of chemical and mineralogical parameters

The addition of different oxidant species to the glass pot is sometimes suggested to enhance the oxidizing state of the melt. Besides nitrates (Bontemps, 1868), sulphate is often mentioned as a possible oxidant in historical glasses (Bidegaray et al., 2019), as its thermal decomposition releases O_2 in the melt (Bingham and Jackson, 2008). However, this reaction takes place only if the furnace temperature is over 1400°C, which seems unlikely at the time (Hunault et al., 2017b). The redox state of the melt may be modified by the interaction between Fe and Mn redox couples (Bidegaray et al., 2020; Ferrand et al., 2015; Gliozzo, 2017; Hunault et al., 2017b) according to the reaction:

$$Fe^{2+} + Mn^{3+} \leftrightarrows Fe^{3+} + Mn^{2+} \quad (1)$$

This relation controls the colour of glasses. Indeed, the right side of this equation concerns two ions that do not significantly contribute to this colour, as they have a low molar extinction coefficient. By contrast,

Fe^{2+} and Mn^{3+} are efficient colouring agents (see 4.4). The relative concentration of these two contributions will determine the resulting glass colour. Manganese concentration is always in excess with respect to iron (Fig. 8), as in other medieval glasses (Adlington et al., 2019; Bidegaray et al., 2019; Hunault et al., 2021). However, the Mn^{3+}/Mn_{total} ratio is not correlated with the Mn/Fe ratio of the glass (Fig. 8), suggesting that other factors may influence the final concentration of Mn^{3+} in the glass, through the use of oxidized Mn-minerals.

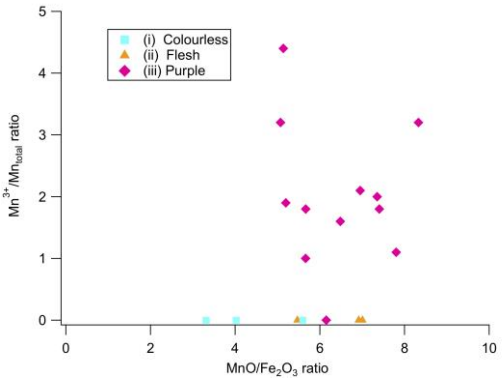

Fig. 8: Evolution of the percentage of Mn occurring as Mn^{3+} in the glasses as a function of the molar ratio MnO/Fe_2O_3. On a molar basis, Mn is clearly in excess relative to Fe. The relative Mn^{3+} content, which is only detectable in purple glasses, does not show any clear chemical dependence.

These minerals are usually manganese oxides, easy to collect as they are ubiquitous at the Earth's surface where they are found in soils and ore deposits and used over centuries to make colourless or purple glasses, as described by Neri (in Cable, 2006). They occur as intimately intermixed mineral mixtures with oxidized Mn^{3+} and Mn^{4+} (Post, 1999). The most frequently evocated minerals are pyrolusite, MnO_2 (Mn^{4+}) and "psilomelane". Though this latter is often mentioned as a possible Mn source since Roman glasses (Silvestri, 2008), it is actually not a mineral but a complex mixture with predominantly the mineral romanechite ($Ba_{0.66}$ Mn_5 O_{10} .1.34 H_2O) containing both Mn^{3+} and Mn^{4+} (Post, 1999). A recent experimental work (Bidegaray et al., 2019) suggests that the oxidation state of manganese in raw materials plays a role in the efficiency of the mutual Mn-Fe redox interactions during glass making.

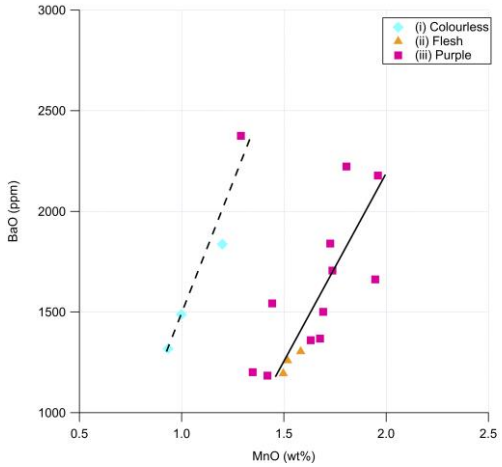

Fig. 9. Biplot showing the concentration of Mn and Ba. The lines show the linear regressions calculated for two groups, the colourless glasses (goodness of fit: r=0.9) and the purple and flesh-coloured glasses (r=0.82).

Wood-ash glasses show a positive correlation between Mn and Ba (e.g., Gallo et al., 2013; Van Wersch et al., 2015), also observed in Roman coloured glasses (e.g., Silvestri, 2008). An original finding of the present study is that this Mn-Ba correlation (Fig. 9) follows two different trends corresponding to flesh-coloured and purple glasses and to colourless glasses. This suggests two different sources of manganese, one being enriched in barium (blue line) relative to the other (red line). Figure 9 also shows that the glasses using the hypothetical manganese source enriched in barium are also the poorest in total manganese. They come from Sainte-Chapelle, Saint-Germain-des-Prés and Normandy and are the most recent glasses of the corpus (Supplementary Fig. S5). Barium is associated to Mn^{3+}-Mn^{4+} oxide minerals as romanechite, psilomelane being a discredited mineral mixture (see above). This allows use Ba to trace the Mn-minerals used for glassmaking. In order to obtain a purple or flesh-coloured glass, glassmakers may have intentionally added manganese minerals in the pot, using another manganese source. This may be the case of pyrolusite or wad, a Mn^{3+}-Mn^{4+} oxide mineral mixture devoid of barium (Post, 1999). Similarly, in the 15th century glass of the Rose of the Sainte Chapelle in Paris, Mn and Ba concentrations follow two different trends depending on whether the glass is purple or not, which would mean that two different sources of manganese were used (Hunault et al., 2017a and 2021).

4.7. Control of the redox conditions: Importance of the kinetic effects

Earlier work recognized the importance of controlling the atmosphere of the furnace by ancient glassmakers (Bontemps, 1868). For instance, a 15th-century glass of Sainte Chapelle, associates different colours, prepared under reducing or oxidizing conditions for the red and colourless glasses, and the deep purple glasses, respectively (Hunault et al., 2017). This control may be achieved by modifying the air flux within the furnace, as suggested by Monk Theophilus for the design of medieval furnaces (Hawthorne and Smith, 1979). The feasibility of the control of the firing atmosphere was demonstrated by an experimental work based on the construction and operation of a replica of a medieval furnace (Royce-Roll, 1994). However, it is easier to create reducing than oxidizing conditions in furnaces fuelled with wood, as observed in cobalt-containing medieval blue glasses with pO_2 of the order of 10^{-8} bar (Hunault et al., 2016a). Such a reducing atmosphere is incompatible with the presence of Mn^{3+} (Schreiber, 1986).

It is unlikely that the melting atmosphere was adjusted to these contrasted conditions, given what we know about medieval glass furnaces (Bingham and Jackson, 2008; Sellner et al., 1979). This rather indicates that the manganese redox equilibrium has not been reached and that the purple colour is a transient state between the high oxidation state of Mn in the raw materials and that in the glass. It is well known that Fe^{2+} and Mn^{3+} do not coexist in glasses at equilibrium, as illustrated by reaction (1). This efficient redox interaction (Bidegaray et al., 2020; Ferrand et al., 2015; Gliozzo, 2017) is based on electron exchange between the two Fe^{2+}/Fe^{3+} and Mn^{2+}/Mn^{3+} redox couples, a process faster than the equilibration with molecular dioxygen from the furnace atmosphere (Chopinet et al., 2002). Generating oxidizing conditions able to stabilize Mn^{3+} imply out of equilibrium conditions. Indeed, kinetic effects play a major role in glass making, at the melting and fining stages: the Fe^{2+}/Fe^{3+} redox equilibrium of potassic (alumino)silicate melts with the furnace atmosphere is achieved after 12 h at 1400°C (Dickenson and Hess, 1982), as it takes about 20 h at this temperature for a 2 mm-thick sodium silicate melt (Paul, 1990). The Fe equilibrium redox state in a larger batch is obtained at even longer melting durations: in a 2 cm-thick melt, melting duration needs about 60 h to reach the equilibrium, despite regularly stirring the melt (Supplementary Fig. S6). Indeed, the diffusion coefficient of molecular oxygen in a silicate melt is low, about 6.9×10^{-8} cm^2/s and 3.7×10^{-7} cm^2/s in potassic and sodic/soda-lime melts at 1260°C, respectively. This supports the interpretation of the redox equilibrium as being a diffusion-dependent process (Goldman and Gupta, 1983). A direct consequence is that the chemical diffusion throughout the melt limits the influence of the furnace atmosphere (Bidegaray et al., 2020).

When using raw materials as Fe^{3+}- and Mn^{3+}-Mn^{4+}-oxides, in which these elements are already oxidized, the slow attainment of the equilibration of redox equilibria in silicate melts implies that shorter the melting

time, the more oxidized will be resulting glass. With increasing temperature, the raw Mn oxide minerals remain in a high oxidation state, as in Mn_3O_4, a mixed Mn^{3+}-Mn^{2+} oxide that is stable above 1000°C (see e.g. Chu et al., 2021), i.e. during the first stages of melting. In that case, a rapid processing followed by a fast blowing will ensure a high proportion of oxidized Mn^{3+} be retained in the glass.

5. Conclusion

The analysed corpus of medieval stained glasses representing character heads is of major historical and artistic interest. It provides an overview of glassmaking techniques in 12th -15th centuries. The compositional variability of the elemental concentrations of the major glass components remains limited, similar to that found for single monuments despite the diversity of geographic origins. These heads present a noteworthy diversity and originality of hues, able to describe skin colour, from almost colourless bluish to intense purple, through flesh-tone, a colour that is exclusive to the depiction of skin complexion. This variety of colours comes mainly from the relative amounts of Fe^{2+} or Mn^{3+} ions. These efficient colouring agents cannot coexist in the molten glass, which ensures some colour purity. When Fe^{2+} is in excess, the glass has a slight blue to green tint. When Mn^{3+} is in excess, glass colour ranges from pinkish to purple. The intermediate situation favours the weakly colouring forms Fe^{3+} and Mn^{2+} species, which provide a slight flesh-tone tint.

Manganese speciation, and in particular the Mn^{3+}/Mn_{total} ratio, determines the flesh-tone to purple colour, despite the low relative abundance of oxidized manganese. Indeed, Mn^{2+} remains the majority Mn oxidation state in all glasses (at least 95% total Mn). There is no evidence of the addition of an extra oxidant in the glass pot. The mastering of purple glass production required unusual oxidizing conditions, mostly by adjusting the kinetics of the glass making process, taking advantage of the use of raw materials containing oxidized Mn- and Fe-oxide minerals. The influence of the atmosphere is limited by the slow diffusion of molecular oxygen within the melt. This favours the hypothesis of a short duration of melting and fining, in order to favour an oxidized redox state of manganese in out of equilibrium conditions. The difficulty to control the making of purple glasses explains their relative scarcity. For instance, they represent only about 20 and 10% of the total surface of the stained glass windows in the Nave of the Sainte-Chapelle in Paris and the Rose of Cathedral of Reims, respectively (Capobianco et al., 2020; Hunault et al., 2021). These technical difficulties may also be responsible of the large variability of hues used to represent skin complexion in this corpus. Our results support the point of view of Royce-Roll (1994), who stated that: "It is my belief that the colouring process prior to the 13th century was more difficult to control for certain colours, and thus limited the palette used during this period". Flesh-tone may have been one of these colours.

Declaration of Competing Interest The authors declare that they have no known competing financial interests or personal relationships that could have appeared to influence the work reported in this paper.

Acknowledgments

We gratefully acknowledge the AGLAE team of C2RMF coordinated by Claire Pacheco, the SOLEIL Synchrotron and the team of the LUCIA beamline. We thank two anonymous reviewers for their fruitful suggestions that improved the manuscript. This work has been supported by the University Institute of France.

Appendix A.

Figure A1. Medieval character heads analysed by PIXE/PIGE. The estimate of the dates and origin is from Lautier and Boulanger (2009).

557 Brief description of the Medieval character heads analysed by PIXE/PIGE (H: height, W: width).

41 C and F (Cap and Face, respectively). Saint-Pierre and Saint-Paul Cathedral, Poitiers, 1165: Head of a bearded man, Bay 102; H. 11.6 cm; W. 8.5 cm. Window on the life of Saint Peter (piece of glass placed as a filler in a half medallion).

47-10. Saint-Maurice Cathedral, Angers, 1190-1210: Head of a bearded King or Bishop; H. 10.2 cm; W. 10.2 cm. Elaboration linked to the production of the Angevin workshop of the Master of Saint Martin.

47-23. Ibid: Head of an executioner; H. 5 cm; W. 10 cm. Linked to the production of the Angevin workshop of the Master of Saint Martin.

47-17. Ibid, 1230-1235: Head of a bearded man, Bay: 127 (formerly b. 126); H. 8. 5 cm; W. 8.2 cm.

42-2. Chartres Cathedral, 1200-1205: Head of a flying angel, Bay 42, Panel 62; H. 7.7 cm; W. 6.5 cm.

43-2. Ibid.: Head of a bearded man, Bay 42, panel 28; H. 9.5 cm; W. 7.5 cm. Window of the Death and Glorification of the Virgin.

47-8. Saint Stephen Cathedral of Bourges, 1210-1215: Angel's head, Bay: 4, panel 32; H. 12 cm; W. 8 cm. Window of the Last Judgment: angel holding the instruments of the Passion.

47-25. Ibid.: Man's head, Bay: 23, panel 21; H. 8.5 cm; W. 6.5 cm. Stained glass of Lazarus: death of the bad rich man. Elaborated by the workshop of the Master of Saint Stephen relics, a workshop active in Bourges in the first third of the 13th century.

44-2. Ibid.: Head of a bearded man, Bay: 20, panel 13 or 14; H. 8.4 cm; W. 6.6 cm. Window of the life of Saint John the Baptist.

47-1. Sainte-Chapelle, Paris, 1243-1248: Head of a young man, Bay H, Passion of Christ, panel 81; H. 9.4 cm; W. 7.5 cm. Window of the Crown of thorns.

47-5 C and F (crown and face, respectively). Ibid.: King's head, Bay D or E; H. 12.5 cm; W. 8.6 cm.

44-3. Abbey Church of Saint-Germain-des-Prés, Chapel of the Virgin, Paris, 1245-1247: Bishop Valerius (on the left) and Saint Vincent chained (on the right); H. 14.5 cm; W. 8.3 cm. Window on the Life and history of the relics of Saint Vincent of Zaragoza (now at Metropolitan Museum, New York, G. Dupont Pratt donation).

42-5. Ibid.: Angel's head; H. 6.2 cm; W. 5.5 cm. Bay on the Life and history of the relics of Saint Vincent of Zaragoza (now at Metropolitan Museum, New York, G. Dupont Pratt donation)

43-1. Cathedral of Soissons, 1200-1225: Head of a bearded man; H. 9.5 cm; W. 7.5 cm.

44-1. Soissons Cathedral or Collegiate church of Saint-Quentin, 1200-1233: Head of a sleeping man; H. 13.8 cm; W. 10 cm. Window of Saint John the Evangelist.

42-3. Sens Cathedral, around 1230: Head of a man, Bay 1 probable; H. 10.5 cm; W. 8 cm.

47-28. Church of Notre-Dame, Dives/Mer, before 1336: Angel's head, Bay 0 in the Tympanum; H. 10 cm; W. 7 cm.

Appendix B.

		Purple										*Flesh*					*Colourless*				*Yellow*
	Glass	41C	41F	42-3	43-1	43-2	44-1	44-2	47-1	47-5F	47-8	47-17	47-25	42-2	47-10	47-23	42-5	44-3	47-28	47-5C
SiO_2	A	59.95	57.48	57.06	55.26	57.60	57.55	57.49	53.99	55.87	56.31	56.67	55.02	57.90	61.71	60.56	59.42	60.04	59.70	56.91
	±σ	*0.14*	*0.28*	*0.23*	*0.56*	*0.24*	*0.30*	*0.47*	*0.12*	*0.12*	*0.23*	*0.47*	*0.70*	*0.13*	*0.36*	*0.06*	*0.14*	*0.09*	*0.14*	*0.45*
Na_2O	A	0.85	0.81	0.73	0.45	1.76	0.75	0.75	0.63	0.90	0.68	1.24	0.51	1.66	0.87	0.96	0.74	1.62	2.29	0.70
	±σ	*0.01*	*0.01*	*0.02*	*0.02*	*0.06*	*0.02*	*0.06*	*0.04*	*0.06*	*0.03*	*0.05*	*0.02*	*0.03*	*0.05*	*0.01*	*0.01*	*0.02*	*0.00*	*0.02*
K_2O	A	14.89	15.84	14.91	16.60	12.66	17.05	15.67	17.11	14.40	15.38	14.61	17.95	13.24	13.29	13.46	13.79	14.37	13.53	16.94
	±σ	*0.09*	*0.05*	*0.09*	*0.37*	*0.10*	*0.13*	*0.34*	*0.10*	*0.08*	*0.07*	*0.08*	*0.46*	*0.06*	*0.15*	*0.10*	*0.06*	*0.10*	*0.03*	*0.08*
CaO	A	12.59	13.35	13.37	13.77	14.46	10.44	12.74	13.38	13.77	13.65	14.01	12.60	13.90	12.25	12.59	12.96	11.00	11.67	11.99
	±σ	*0.05*	*0.22*	*0.02*	*0.34*	*0.15*	*0.04*	*0.28*	*0.03*	*0.04*	*0.02*	*0.13*	*0.23*	*0.04*	*0.10*	*0.02*	*0.11*	*0.04*	*0.04*	*0.18*
MgO	A	3.63	3.63	5.35	4.58	4.98	4.81	3.91	5.04	5.97	5.35	5.61	4.00	5.13	4.08	4.49	4.55	6.55	5.97	4.48
	±σ	*0.10*	*0.10*	*0.07*	*0.07*	*0.08*	*0.13*	*0.18*	*0.09*	*0.09*	*0.17*	*0.20*	*0.16*	*0.05*	*0.11*	*0.05*	*0.06*	*0.03*	*0.21*	*0.01*
Al_2O_3	A	2.03	1.87	1.52	1.44	1.78	1.99	1.50	1.21	1.74	1.45	1.71	1.35	1.70	1.70	1.59	2.21	1.21	1.25	1.75
	±σ	*0.04*	*0.04*	*0.03*	*0.01*	*0.02*	*0.04*	*0.04*	*0.02*	*0.00*	*0.01*	*0.14*	*0.02*	*0.02*	*0.12*	*0.03*	*0.04*	*0.03*	*0.04*	*0.04*
P_2O_5	A	2.92	3.48	3.36	4.14	3.15	3.53	3.72	4.88	4.07	3.60	2.28	5.11	3.01	2.66	2.99	2.76	2.27	3.01	3.79
	±σ	*0.10*	*0.08*	*0.09*	*0.03*	*0.00*	*0.05*	*0.13*	*0.05*	*0.00*	*0.00*	*0.15*	*0.04*	*0.00*	*0.03*	*0.08*	*0.04*	*0.01*	*0.09*	*0.09*
SO_3	A	0.26	0.31	0.23	0.31	0.19	0.23	0.48	0.36	<0.16	0.19	0.25	0.46	0.25	0.36	0.33	0.27	<0.11	0.10	0.42
	±σ	*0.04*	*0.04*	*0.03*	*0.08*	*0.02*	*0.03*	*0.08*	*0.04*	*0.04*	*0.03*	*0.01*	*0.07*	*0.03*	*0.03*	*0.04*	*0.07*	*0.05*	*0.01*	*0.08*
Cl	A	0.40	0.46	0.39	0.37	0.45	0.43	0.45	0.51	0.40	0.39	0.35	0.40	0.53	0.41	0.39	0.35	0.52	0.54	0.41
	±σ	*0.01*	*0.02*	*0.01*	*0.00*	*0.00*	*0.01*	*0.01*	*0.00*	*0.01*	*0.02*	*0.01*	*0.02*	*0.00*	*0.02*	*0.01*	*0.00*	*0.01*	*0.01*	*0.01*
Fe_2O_3	A	0.58	0.62	0.56	0.60	0.65	0.75	0.56	0.51	0.51	0.55	0.53	0.53	0.62	0.51	0.49	0.81	0.40	0.52	0.52
	±σ	*0.01*	*0.00*	*0.02*	*0.02*	*0.01*	*0.01*	*0.02*	*0.00*	*0.01*	*0.00*	*0.01*	*0.01*	*0.02*	*0.02*	*0.01*	*0.02*	*0.01*	*0.01*	*0.01*
MnO	A	1.35	1.42	1.74	1.73	1.63	1.69	1.95	1.68	1.29	1.81	1.96	1.44	1.50	1.58	1.52	1.20	1.00	0.93	1.19
	±σ	*0.02*	*0.01*	*0.04*	*0.08*	*0.01*	*0.01*	*0.06*	*0.06*	*0.04*	*0.01*	*0.01*	*0.01*	*0.06*	*0.07*	*0.02*	*0.02*	*0.01*	*0.02*	*0.02*
CoO	A	<0.001	<0.002	<0.005	<0.005	0.009	<0.004	<0.006	<0.003	<0.001	<0.006	<0.006	<0.006	0.007	<0.002	<0.002	0.006	<0.002	<0.004	<0.003
	±σ	*0.001*	*0.000*	*0.001*	*0.000*	*0.001*	*0.001*	*0.000*	*0.001*	*0.001*	*0.000*	*0.000*	*0.000*	*0.000*	*0.000*	*0.000*	*0.002*	*0.000*	*0.000*	*0.000*
NiO	A	0.002	0.002	0.003	0.004	0.006	0.004	0.004	0.002	0.002	0.004	0.004	0.003	0.005	0.001	0.002	0.003	0.001	0.003	0.002
	±σ	*0.000*	*0.000*	*0.000*	*0.000*	*0.000*	*0.000*	*0.000*	*0.000*	*0.000*	*0.000*	*0.000*	*0.000*	*0.000*	*0.000*	*0.000*	*0.000*	*0.000*	*0.000*	*0.000*
CuO	A	0.007	0.023	0.173	0.042	0.040	0.028	0.024	0.026	0.036	0.022	0.067	0.023	0.020	0.010	0.012	0.103	0.202	0.034	0.025
	±σ	*0.000*	*0.001*	*0.005*	*0.001*	*0.001*	*0.000*	*0.001*	*0.001*	*0.001*	*0.000*	*0.002*	*0.001*	*0.001*	*0.000*	*0.001*	*0.003*	*0.003*	*0.001*	*0.001*
ZnO	A	0.027	0.033	0.048	0.034	0.063	0.041	0.053	0.034	0.036	0.046	0.046	0.069	0.044	0.039	0.045	0.045	0.056	0.028	0.037
	±σ	*0.001*	*0.001*	*0.001*	*0.002*	*0.000*	*0.001*	*0.009*	*0.000*	*0.001*	*0.001*	*0.001*	*0.005*	*0.001*	*0.002*	*0.001*	*0.001*	*0.001*	*0.001*	*0.001*
TiO_2	A	0.25	0.26	0.19	0.26	0.23	0.27	0.19	0.21	0.25	0.18	0.16	0.18	0.23	0.21	0.20	0.28	0.13	0.11	0.23
	±σ	*0.01*	*0.00*	*0.00*	*0.01*	*0.00*	*0.01*	*0.01*	*0.01*	*0.01*	*0.00*	*0.00*	*0.00*	*0.01*	*0.01*	*0.00*	*0.01*	*0.00*	*0.00*	*0.01*
PbO	A	0.07	0.19	0.09	0.13	0.10	0.17	0.21	0.19	0.23	0.05	0.15	0.09	0.04	0.09	0.16	0.14	0.24	0.10	0.23
	±σ	*0.03*	*0.03*	*0.01*	*0.07*	*0.01*	*0.01*	*0.05*	*0.04*	*0.05*	*0.01*	*0.03*	*0.02*	*0.01*	*0.01*	*0.03*	*0.01*	*0.02*	*0.00*	*0.04*
Rb_2O	A	0.016	0.018	0.023	0.015	0.017	0.024	0.026	0.025	0.029	0.022	0.024	0.029	0.016	0.017	0.017	0.025	0.024	0.020	0.033
	±σ	*0.000*	*0.000*	*0.000*	*0.001*	*0.000*	*0.000*	*0.000*	*0.001*	*0.001*	*0.000*	*0.001*	*0.000*	*0.001*	*0.001*	*0.000*	*0.001*	*0.001*	*0.000*	*0.000*
SrO	A	0.031	0.035	0.055	0.043	0.042	0.049	0.059	0.042	0.076	0.067	0.076	0.054	0.039	0.040	0.039	0.064	0.078	0.035	0.069
	±σ	*0.001*	*0.001*	*0.002*	*0.001*	*0.001*	*0.001*	*0.001*	*0.001*	*0.001*	*0.000*	*0.000*	*0.000*	*0.001*	*0.001*	*0.002*	*0.001*	*0.001*	*0.001*	*0.002*
ZrO_2	A	0.021	0.020	0.012	0.025	0.023	0.019	0.012	0.015	0.016	<0.011	<0.011	0.014	0.020	0.016	0.017	0.019	<0.009	0.008	0.018
	±σ	*0.001*	*0.000*	*0.001*	*0.003*	*0.002*	*0.000*	*0.002*	*0.000*	*0.002*	*0.001*	*0.000*	*0.001*	*0.001*	*0.002*	*0.001*	*0.001*	*0.001*	*0.002*	*0.001*
BaO	A	0.12	0.12	0.17	0.18	0.14	0.15	0.17	0.14	0.24	0.22	0.22	0.15	0.12	0.13	0.13	0.13	0.18	0.15	0.13	0.23
	±σ	*0.01*	*0.02*	*0.01*	*0.01*	*0.01*	*0.01*	*0.01*	*0.01*	*0.01*	*0.01*	*0.00*	*0.01*	*0.01*	*0.00*	*0.00*	*0.01*	*0.02*	*0.01*	*0.01*
Total		99.99	99.97	99.97	99.98	99.97	99.98	99.97	99.98	99.83	99.97	99.96	99.98	99.99	99.98	99.98	99.95	99.85	99.97	99.99

562 **Table B1**.

563 Composition (in wt.%) of the medieval glasses analysed with PIXE/PIGE. A is the average value, σ is the standard
564 deviation, N.D. stands for Not Detected (value under LOD) and < means the value is lower than 3.3LOD. Other
565 elements may have been present in the composition : Cr_2O_3, SnO_2, Sb_2O_5, Ag, Nd_2O_3, V_2O_3, Ga_2O_3, As_2O_5, Y_2O_3,
566 MoO_3, In_2O_3, La_2O_3 and Bi_2O_3 ; when detected their values were lower than 3.3LOD. For the glass #41, the names 41C
567 and 41F designate the cap and face (different shape of purple), respectively. For the glass #47-5, the names 47-5C and
568 47-5F designate the crown (yellow) and face (purple), respectively. The analysis of sample # 47-28 was performed on
569 an unpainted portion of the glass.
570

571

572 **Appendix C.**

573

Glasses	Y	*x*	*y*	L*	a*	b*
Purple						
41C*	0.82	0.398	0.331	7.38	8.16	3.13
42-3	7.79	0.389	0.347	33.55	12.01	9.57
43-1	6.02	0.369	0.330	29.46	10.83	4.55
43-2*	3.46	0.377	0.350	21.79	7.06	6.84
44-1	6.61	0.400	0.328	30.91	17.46	6.97
44-2	0.73	0.395	0.359	6.60	4.43	4.24
47-1	7.10	0.380	0.362	32.03	7.03	10.82
47-8	22.55	0.366	0.368	54.60	4.66	15.51
47-17*	8.26	0.376	0.374	34.53	4.03	13.09
47-25*	24.14	0.398	0.384	56.22	9.20	24.30
Flesh-tone						
41F*	19.69	0.370	0.353	51.49	9.73	12.08
42-2*	10.98	0.382	0.390	39.54	2.26	17.97
47-5F*	39.13	0.354	0.347	68.84	8.91	11.03
47-10*	0.36	0.318	0.303	3.29	1.45	-0.82
47-23*	2.24	0.381	0.359	16.71	5.31	7.13
Colourless						
42-5*	23.80	0.330	0.377	55.88	-8.39	13.11
44-3	50.21	0.306	0.350	76.20	-10.78	5.28
47-28	11.23	0.430	0.494	39.97	-7.01	46.38
Yellow						
47-5C	15.13	0.438	0.447	45.82	2.66	40.69
47-28Y	24.03	0.327	0.363	56.12	-5.38	9.55

574

575 **Table C1.** Colorimetric coordinates of the medieval glasses analysed in PIXE/PIGE, in Y*xy* and L*a*b*
576 system, calculated for the real sample thickness by the method described in 3.3, using the D65 illuminant.
577 The analysis of Sample 47-28 was made both on an unpainted and on a painted portion of the glass.
578 Coordinates of other glasses is given in Supplementary Table T2. The samples chosen to be analysed by
579 XANES spectroscopy are designated by an asterisk.

580

581 The glasses analysed are not fully translucent, mostly because of light scattering due to the alteration of the
582 glass surface. This slight opacity causes which results in overestimating the overall absorbance, hence *Y*
583 values are underestimated. As scattering is isoenergetic, the shape of the spectrum is however preserved, so
584 the *x* and *y* values for chromaticity are correctly evaluated.

585

586

Appendix D. Supplementary information

Supplementary information to this article can be found online at https://doi.org/…

References

Abuin, M., Serrano, A., Chaboy, J., Garcia, M.A., Carmona, N., 2013. XAS study of Mn, Fe and Cu as indicators of historical glass decay. J. Anal. At. Spectrom., 28, 1118-1124. https://doi.org/10.1039/c3ja30374h.

Adlington, L.W., Freestone, I.C., 2017. Using handheld pXRF to study medieval stained glass: A methodology using trace elements. MRS Adv., 2 (2017), 1785-1800. DOI: https://doi.org/10.1557/adv.2017.233.

Adlington, L.W., Freestone, I.C., Kunicki-Goldfinger, J.J., Ayers, T., Gilderdale Scott, H., Eavis, A., 2019. Regional patterns in medieval European glass composition as a provenancing tool. J. Archaeol. Sci. 110, 104991. https://doi.org/10.1016/j.jas.2019.104991.

Aerts, A., Velde, B., Janssens, K., Dijkman, W., 2003. Change in silica sources in Roman and post-Roman glass. Spectrochim. Acta B, 58, 659-667. https://doi.org/10.1016/S0584-8547(02)00287-2.

Arletti, R., Dalconi, M.C., Quartieri, S., Triscari, M., Vezzalini, G., 2006. Roman coloured and opaque glass: a chemical and spectroscopic study. Appl. Phys. A 83, 239e245. https://doi.org/10.1007/s00339-006-3515-2.

Arletti, R., Quartieri, S., Freestone, I.C., 2013. A XANES study of chromophores in archaeological glass. Appl. Phys. A 111, 99–108. https://doi.org/10.1007/s00339-012-7341-4.

Bamford, C.R., 1977. Colour generation and control in glass. Elsevier Scientific Publishing Company : distributors for the U.S. and Canada, Elsevier North-Holland. https://doi.org/10.1002/col.5080030317.

Barrera, J., Velde, B.A., 1989. Study of French medieval glass composition. J. Glass Stud. 31, 48–54. http://www.jstor.org/stable/24190095.

Basso, E., Riccardi, M.P., Messiga, B., Mendera, M., Gimeno, D., García-Vallés, M., Fernandez-Turiel, J.L., Bazzocchi, F., Aulinas, M., Tarozzi, C., 2009. Composition of the base glass used to realize the stained glass windows by Duccio di Buoninsegna (Siena Cathedral, 1288–1289 AD): A geochemical approach. Mater. Charact 60, 1545–1554. https://doi.org/10.1016/j.matchar.2009.09.005.

Bidegaray, A.-I., Godet, S., Bogaerts, M., Cosyns, P., Nys, K., Terryn, H., Ceglia, A., 2019. To be purple or not to be purple? How different production parameters influence colour and redox in manganese containing glass. J. Archaeol. Sci.: Rep. 27, 101975. https://doi.org/10.1016/j.jasrep.2019.101975.

Bidegaray, A.-I., Nys, K., Silvestri, A., Cosyns, P., Meulebroeck, W., Terryn, H., Godet, S., Ceglia, A., 2020. 50 shades of colour: how thickness, iron redox and manganese/antimony contents influence perceived and intrinsic colour in Roman glass. Archaeol. Anthropol. Sci. 12, 109 https://doi.org/10.1007/s12520-020-01050-0.

626 Bingham, P.A., Jackson, C.M., 2008. Roman blue-green bottle glass: chemical–optical analysis and
627 high temperature viscosity modelling. J. Archaeol. Sci. 35, 302–309.
628 https://doi.org/10.1016/j.jas.2007.03.011.
629 Bingham, K., Parke, S., 1965. Absorption and fluorescence spectra of divalent manganese in glasses.
630 Phys. Chem. Glasses 6, 224-232.
631 Biron, I., Verità, M., 2012. Analytical investigation on Renaissance Venetian enamelled glasses from
632 the Louvre collections. J. Archaeol. Sci. 39, 2706-2713. https://doi.org/10.1016/j.jas.2012.03.014.
633 Bontemps, G., 1868. Guide du verrier : traité historique et pratique de la fabrication des verres,
634 cristaux, vitraux (Librairie du "Dictionnaire des arts et manufactures", Paris, 1868).
635 http://gallica.bnf.fr/ark:/12148/bpt6k5663541p. English translation edited by the Society of Glass
636 Technology.
637 Brems, D., Degryse, P., 2014. Trace element analyses in provenancing Roman glass-making.
638 Archaeometry 56, 116-136. https://doi.org/10.1111/arcm.12063
639 Brill, R.H., Pongracz, P., 2004. Stained Glass from Saint-Jean-des-Vignes (Soissons) and
640 Comparisons with Glass from Other Medieval Sites. J. Glass Stud. 46, 115–144.
641 http://www.jstor.org/stable/24190935.
642 Cable M., 2006. The world's most famous book on glassmaking. The Art of Glass by Antonio Neri,
643 translated into English by Christopher Merrett. The Society of Glass Technology.
644 Calas, G., Cormier, L., Galoisy, L., Jollivet, P., 2002. Structure-property relationships in
645 multicomponent oxide glasses. C. R. Chimie, 5, 831-843. https://doi.org/10.1016/S1631-0748(02)01459-5.
646 Calligaro, T., 2008. PIXE in the study of archaeological and historical glass. X-Ray Spectrom. 37,
647 169–177. https://doi.org/10.1002/xrs.1063.
648 Capobianco, N., 2018. La couleur des vitraux au XIIIème siècle. Etude chimique et spectroscopique.
649 Thesis, Sorbonne Université. https://tel.archives-ouvertes.fr/tel-02495688.
650 Capobianco, N., Hunault, M.O.J.Y., Balcon-Berry, S., Galoisy, L., Sandron, D., Calas, G., 2019. The
651 Grande Rose of the Reims Cathedral: an eight-century perspective on the colour management of medieval
652 stained glass. Sci. Rep. 9, 3287. https://doi.org/10.1038/s41598-019-39740-y.
653 Ceglia, A., Nuyts, G., Meulebroeck, W., Cagno, S., Silvestri, A., Zoleo, A., Nys, K., Janssens, K.,
654 Thienpont, H., Terryn, H., 2015. Iron speciation in soda- lime-silica glass: a comparison of XANES and UV-
655 vis-NIR spectroscopy. J. Anal. At. Spectrom. 30, 1552–1561. https://doi.org/10. 1039/c5ja00046g.
656 Chalmin, E., Farges, F., Brown, G. E., 2009. A pre-edge analysis of Mn K-edge XANES spectra to
657 help determine the speciation of manganese in minerals and glasses. Contrib. Mineral. Petrol. 157, 111–126.
658 https://doi.org/10.1007/s00410-008-0323-z.

Chopinet, M.H., Lizarazu, D., Rocanière, C., 2002. L'importance des phénomènes d'oxydoréduction dans le verre. Comptes-rendus de Chimie 5, 939-949. https://doi.org/10.1016/S1631-0748(02)01455-8.

Choudhury, S., Hormes, Agyeman-Budu, D.N., Woll, A.R., George, G.N., Coulthar, I., Pickering I.J., 2015. Application of a spoked channel array to confocal X-ray fluorescence imaging and X-ray absorption spectroscopy of medieval stained glass. J. Anal. At. Spectrom., 30, 759-766. https://doi.org/10.1039/c4ja00389f.

Chu, J., Bao, Y., Li, X., Gao, F., Wang, M., 2021.Characterization of oxidation behavior of Mn fumes generated in the vacuum treatment of melting Mn steels. Steel Res. Int. 92, 2000333. https://doi.org/10.1002/srin.202170011.

De Ferri, L., Arletti, R., Ponterini, G. and Quartieri, S., 2011. XANES, UV-VIS and luminescence spectroscopic study of chromophores in ancient HIMT glass. Eur. J. Mineral. 23, 969–80. https://doi.org/10.1127/0935-1221/2011/0023-2125.

Dickenson, M.P., Hess, P.C., 1986. The structural role and homogeneous redox equilibria of iron in peraluminous, metaluminous and peralkaline silicate melts. Contr. Mineral. Petrol. 92, 207–217.https://doi.org/10.1007/BF00375294.

Ferrand, J., Rossano, S., Loisel, C., Trcera, N., van Hullebusch, E.D., Bousta, F., Pallot-Frossard, I., 2015. Browning phenomenon of medieval stained glass windows. Anal. Chem. 87, 3662–3669. https://doi.org/10.1021/ac504193z.

Gallo, F., Silvestri, A., Molin, G., 2013. Glass from the archaeological museum of Adria (North-East Italy): new insights into Early Roman production technologies. J. Archaeol. Sci. 40, 2589–2605. http://dx.doi.org/10.1016/j.jas.2013.01.017.

Garcia Vallès, M., Vendrell Saz, M., 2002. The glasses of the transept's rosette of the Cathedral of Tarragona: Characterization, classification and decay. Bol. Soc. Esp. Cerám. Vidrio 41, 217–224. http://dx.doi.org/10.3989/cyv.2002.v41.i2.681.

Gimeno, D., Garcia-Valles, M., Fernandez-Turiel, J.L., Bazzocchi, F., Aulinas, M., Pugès, M., Tarozzi, C., Riccardi, M.P., Basso, El, Fortina, C., Mendera, M., Messiga, B., 2008. From Siena to Barcelona: deciphering colour recipes of Na-rich Mediterranean stained glass windows at the XIII-XIV century transition. J. Cult. Herit. 9, 10–15. https://doi.org/10.1016/j.culher.2008.08.001.

Gliozzo, E., 2017. The composition of colourless glass: a review. Archaeol. Anthropol. Sci. 9, 455–483. https://doi.org/10.1007/s12520-016-0388-y.

Goldman, D.S., Gupta, P.K., 1983. Diffusion-controlled redox kinetics in a glassmelt. J. Am. Ceram. Soc. 66, 188-190. https://doi.org/10.1111/j.1151-2916.1983.tb10014.x.

691 Hawthorne, J.G., Smith, C.S., 1979. Theophilus on Divers Arts: the foremost medieval treatise on
692 painting, glassmaking and metal-work. Translated from the Latin with introduction and notes, Dover
693 Publications, Inc. ed. New York.
694 Henderson, J., 2013. Ancient glass: an interdisciplinary exploration. Cambridge University Press,
695 New York and Cambridge. https://doi.org/10.1017/CBO9781139021883
696 Hérold, M., David, V., Recht R., Walter, M., 2014. Vitrail : Ve-XXIe siècle, Paris : Éditions du
697 patrimoine, Centre des monuments nationaux, 592 pp.
698 Hormes, J., Roy, A., Bovenkamp, G.L., Simon, K., Kim, C.Y., Börste, N., Gai, S, 2013. Medieval
699 glass from the Cathedral in Paderborn: A comparative study using X-ray absorption spectroscopy, X-ray
700 fluorescence, and inductively coupled laser ablation mass spectrometry. Appl. Phys. A 111, 91–97,
701 https://doi.org/10.1007/ s00339-012-7505-2.
702 Hunault, M., Bauchau, F., Loisel, C., Hérold, M., Galoisy, L., Newville, M., Calas, G., Lloyd, I.,
703 2016a. Spectroscopic investigation of the coloration and fabrication conditions of medieval blue glasses. J.
704 Am. Ceram. Soc. 99, 89–97. https://doi. org/10.1111/jace:13783.
705 Hunault, M., Lelong, G., Gauthier, M., Gélébart, F., Ismael, S., Galoisy, L., Bauchau, F., Loisel, C.,
706 Calas, G., 2016b. Assessment of transition element speciation in glasses using a portable transmission
707 ultraviolet–visible–near-Infrared (UV-Vis-NIR) spectrometer. Appl Spectrosc 70, 778–784.
708 https://doi.org/10.1177/ 0003702816638236.
709 Hunault, M.O.J.Y., Loisel, C., Bauchau, F., Lemasson, Q., Pacheco, C., Pichon, L., Moignard, B.,
710 Boulanger, K., Hérold, M., Calas, G., Pallot-Frossard, I., 2017a. Nondestructive redox quantification reveals
711 glassmaking of rare French gothic stained glasses. Anal. Chem. 89, 6277–6284. https://doi.org/10.1021/acs.
712 analchem.7b01452.s001.
713 Hunault, M.O.J.Y., Vinel, V., Cormier, L., Calas, G., 2017b. Thermodynamic insight into the
714 evolution of medieval glassworking properties. J. Am. Ceram. Soc. 100, 2363–2367.
715 https://doi.org/10.1111/jace:14819.
716 Hunault, M.O.J.Y., Loisel, C., 2020. Looking through model medieval green glasses: From color to
717 recipe. Int J Appl Glass Sci 11, 463–470. https://doi.org/10.1111/ ijag.15134.
718 Hunault, M.O.J.Y., Bauchau, F., Boulanger, K., Hérold, M., Calas, G., Lemasson, Q., Pichon, L.,
719 Pacheco, C., Loisel, C., 2021. Thirteenth-century stained glass windows of the Sainte-Chapelle in Paris: An
720 insight into medieval glazing work practices. J. Archaeol. Sci.: Rep. 35, 102753.
721 https://doi.org/10.1016/j.jasrep.2020.102753.
722 Hunt, W. G., , M. R., 1991. Measuring colour, Wiley, Chichester.
723 https://doi.org/10.1002/9781119975595

724 Kunicki-Goldfinger, J. J., Freestone, I. C., McDonald, I., Hobot, J. A., Gilderdale-Scott, H., Ayers, T.,
725 2014. Technology, production and chronology of red window glass in the medieval period – Rediscovery of
726 a lost technology. J. Archaeol. Sci., 41, 89–105. http://dx.doi.org/10.1016/j.jas.2013.07.029.
727 Lautier, C., Sandron, D., 2008. Antoine de Pise: l'art du vitrail vers 1400. Editions du CTHS, Paris.
728 Lautier, C., Boulanger, K. 2009. Rapport d'expertise pour la Réunion des Musées Nationaux. Tech.
729 Rep., Ministère de la Culture et des communications.
730 Lin, Y., Liu, T., Toumazou, M.K., Counts, D.B., Kakoulli, I., 2019. Chemical analyses and
731 production technology of archaeological glass from Athienou-Malloura, Cyprus. J. Archaeol. Sci.: Rep. 23,
732 700-713. https://doi.org/10.1016/j.jasrep.2018.08.011.
733 Meulebroeck, W., Wouters, H., Nys, K., Thienpont, H., 2016. Authenticity screening of stained glass
734 windows using optical spectroscopy. Scientific Reports 6, 37726; https://doi.org/10.1038/srep37726.
735 Möncke, D., Ehrt, D., Kamitsos, E. I, 2013. Spectroscopic study of manganese-containing borate and
736 borosilicate glasses: cluster formation and phase separation. Phys. Chem. Glasses-European J. Glass Sci.
737 Technol. Part B 54, 42–51.
738 Newton, R.G., 1976. Chemical analyses of medieval window glasses - Part 1. Corpus Vitr. Newsl. 21,
739 9–16.
740 Palomar, T., 2018. Chemical composition and alteration processes of glasses from the Cathedral of
741 León (Spain). Bol. Soc. Esp. Ceram. 57, 101-111. https://doi.org/10.1016/j.bsecv.2017.10.001.
742 Palomar, T., Grazia, C., Pombo Cardoso, I., Vilarigues, M., Miliani, C., Romani, A., 2019. Analysis
743 of chromophores in stained- glass windows using Visible Hyperspectral Imaging in- situ. Spectrochim. Acta
744 A 223, 117378. https://doi.org/10.1111/ijag.15611.
745 Paul A., 1990. Oxidation-reduction equilibrium in glass. J. Non-Cryst. Solids 123, 354-362.
746 https://doi.org/10.1016/0022-3093(90)90808-Y.
747 Pichon, L., Calligaro, T., Lemasson, Q., Moignard, B., Pacheco, C., 2015. Programs for visualization,
748 handling and quantification of PIXE maps at the AGLAE facility. Nucl. Instrum. Methods Phys. Res., Sect.
749 B 363, 48–54. https://doi.org/10.1016/j. nimb.2015.08.086.
750 Post, J.E., 1999. Manganese oxide minerals: Crystal structures and economic and environmental
751 significance. Proc. Natl. Acad. Sci. USA 96, 3447-3454. https://doi.org/10.1073/pnas.96.7.3447.
752 Quartieri, S., Triscari, M., Sabatino, G., Boscherini, F., Sani, A., 2002. Fe and Mn K-edge XANES
753 study of ancient Roman glasses. Eur. J. Mineral., 14, 749–756. https://doi.org/10.1127/0935-
754 1221/2002/0014-0749.

Quartieri, S., Riccardi, M.P., Messiga, B., Boscherini, F., 2005. The ancient glass production of the Medieval Val Gargassa glasshouse: Fe and Mn XANES study. J. Non-Cryst. Solids 351, 3013–3022. https://doi.org/10.1016/j.jnoncrysol.2005.06.046.

Ravel, B., Newville, M., 2005. ATHENA, ARTEMIS, HEPHAESTUS: data analysis for X-ray absorption spectroscopy using IFEFFIT. J. Synchrotron Radiat. 12, 537–541. http://doi.org/10.1107/S0909049505012719.

Rehren, T., Brüggler, M., 2015. Composition and production of late antique glass bowls type Helle. J. Archaeol. Sci.: Rep. 3,171-180. http://dx.doi.org/10.1016/j.jasrep.2015.05.021.

Rehren, T., Freestone, I.C., 2015. Ancient glass: from kaleidoscope to crystal ball. J. Archaeol. Sci. 56, 233–241. https://doi.org/10.1016/j.jas.2015.02.021.

Royce-Roll, D., 1994. The colours of romanesque stained glass,-. J. Glass Studies 3, 71–80. http://www.jstor.org/stable/24190054.

Schalm, O., Janssens, K., Wouters, H., Caluwé, D., 2007. Composition of 12–18th century window glass in Belgium: Non-figurative windows in secular buildings and stained- glass windows in religious buildings. Spectrochim. Acta, Part B 62, 663–668. https://doi.org/10.1016/j.sab.2007.03.006.

Schibille, N., Neri, E., Ebanista, C., Ramzi, M., Bisconti, F., 2018. Something old, something new: The late antique mosaics from the catacomb of San Gennaro (Naples). J. Archaeol. Sci. Rep. 20, 411-422. https://doi.org/10.1016/j.jasrep.2018.05.024.

Schreiber, H.D., 1986. Redox processes in glass-forming melts. J. Non-Cryst. Solids 84, 129-141. https://doi.org/10.1016/0022-3093(86)90770-2.

Sellner, C., Oel, H., Camara, B., 1979. Untersuchung alter Gläser (Waldglas) auf Zusammenhang von Zusammensetzung, Farbe und Schmelzatmosphäre mit der Elektronenspektroskopie und der Elektronenspinresonanz (ESR). Glastech. Ber. 52, 255–264.

Silvestri, A., 2008. The coloured glass of Iulia Felix. J. Archaeol. Sci. 35, 1489e1501. https://doi.org/10.1016/j.jas.2007.10.014.

Simmons, C. T., Mysak, L. A., 2010. Transmissive properties of Medieval and Renaissance stained glass in European churches. Archit. Sci. Rev. 53, 251–274. https://doi.org/10.3763/asre.2009.0073.

Simmons, C. T., Mysak, L. A. Stained Glass and Climate Change: How are they Connected?, 2012. Atmos.-Ocean 50, 219–240, https://doi.org/10.1080/07055900.2012.667387.

Smith, R., Carlson, J.H., Newman R.M., 1987. An investigation into the deterioration of painted Limoges enamel plaques c. 1470-1530. Stud. Conserv. 32, 102-113. https://doi.org/10.2307/1506214.

Terczynska-Madej, A., Cholewa-Kowalska, K., Laczka, M., 2010. The effect of silicate network modifiers on colour and electron spectra of transition metal ions. Opt. Mater. 32, 1456–1462. http://doi.org/10.1016/j.optmat.2010.05.024.

Tite, M.S., Pradell, T., Shortland, A.J., 2008. Discovery, production and use of tin-based opacifiers in glasses, enamels and glazes from the Late Iron Age onwards: a reassessment. Archaeometry 50, 67-84. https://doi.org/10.1111/j.1475-4754.2007.00339.x.

Turner, W., Turner, J., 1970. Absorption spectra and concentration dependent luminescence of Mn^{2+} in silicate glasses. J. Am. Ceram. Soc. 53, 329-335. http://doi.org/10.1111/j.1151-2916.1970.tb12118.x.

Van Wersch, L., Loisel, C., Mathis, F., Strivay, D., Bully, S. 2016. Analyses of Early Medieval Stained Window Glass From the Monastery of Baume-Les-Messieurs (Jura, France), Archaeometry, 58, 930-946. ttp://doi.org/10.1016/10.1111/arcm.12207.

Vercamer, V., Lelong, G., Hijiya, H., Kondo, Y., Galoisy, L., Calas, G., 2015. Diluted Fe^{3+} in silicate glasses: Structural effects of Fe-redox state and matrix composition. An optical absorption and X-band/Q-band EPR study. J. Non-Cryst. Solids 428, 138–145. https://doi.org/10.1016/j.jnoncrysol.2015.08.010.

Verità, M., Santopadre, P., 2010. Analysis of gold-colored Ruby glass Tesserae in Roman church mosaics of the fourth to 12th centuries. J. Glass Stud. 52, 1e14.

Vilarigues, M., da Silva, R.C., 2004. Ion beam and infrared analysis of medieval stained glass. Appl. Phys. A 79, 373–378. https://doi.org/10.1007/s00339-004-2538-9.

Vilarigues, M., Coutinho, I., Medici, T., Alves, L.C., Gratuze, B., Machado, A., 2019. From beams to glass: determining compositions to study provenance and production techniques. Phys. Sci. Rev. 4, 0019. https://doi.org/10.1515/psr-2018-0019.

Wedepohl, K.H., Simon, K., 2010. The chemical composition of medieval wood ash glass from Central Europe. Geochemistry 70, 89–97. https://doi.org/10.1016/j.chemer.2009.12.006.

Winterstein-Beckmann, A., Möncke, D., Palles, D., Kamitsos, E. I., Wondraczek, L., 2013. Structure–property correlations in highly modified Sr, Mn-borate glasses. J. Non-Cryst. Solids 376, 165–174. https://doi.org/10.1016/j.jnoncrysol.2013.05.029.

Yamashita, M., Yao, Z., Matsumoto, Y., Utagawa, Y., Kadono, K., Yazawa, T., 2004. X-ray irradiation-induced coloration of manganese in soda-lime silicate glass. J. Non-Cryst. Solids 333, 37–43. https://doi.org/10.1016/j.jnoncrysol.2003.09.040.

Supplementary Information for:

Skin representation in medieval stained glasses: the role of manganese

Natan Capobianco[a], Myrtille O.J.Y. Hunault[b], Claudine Loisel[c,d], Barbara Trichereau[c,d], Fanny Bauchau[c,d,e], Nicolas Trcera[b], Laurence Galoisy[a], Georges Calas[a]

[a]Sorbonne Université, Muséum National d'Histoire Naturelle, UMR CNRS 7590, IRD, Institut de Minéralogie, de Physique des Matériaux et de Cosmochimie, IMPMC, 75005 Paris, France

[b]SOLEIL synchrotron, Gif-sur-Yvette, France

[c]Laboratoire de Recherche des Monuments Historiques, Ministère de la Culture, 77420 Champs-sur-Marne, France

[d]Centre de Recherche sur la Conservation (CRC), Muséum national d'Histoire naturelle, CNRS, Ministère de la Culture, 75005 Paris, France

[e]Centre Interdisciplinaire de Conservation et de Restauration du Patrimoine, Ministère de la Culture, 13003 Marseille, France

Content

Supplementary information A

The historical context of the discovery of these character heads

Our study on the fabrication of purple glasses in the Middle Ages was conducted on a corpus of medieval glasses, called "The Heads". This set consists of 62 pieces of medieval glass, mostly faces of characters, seized by French authorities in 2009 at the occasion of a selling auction at Chartres, on the grounds that these pieces came from public historical monuments owned by the French State and that they were therefore an inalienable property. An expertise led by Claudine Lautier and Karine Boulanger (Lautier and Boulanger, 2009) has identified the history of this corpus. In the 19th century, the primary concern of the restoration of stained glass was to find the legibility of the work, and it was therefore common to remove pieces that were too weathered or broken or even used as fillers in the windows, replacing them with new pieces estimated to better agree with the rest of the panel. In addition, some pieces were also removed and replaced by copies, on the sole grounds that they were beautiful. In all cases, the original pieces were supposed to be returned to the owners of the stained glass, but this was rarely the case, and some of them remained in private collections. The corpus that is the topic of the present study comes from the collection of Dina Vierny (1919-2009), art collector and model and muse for several artists, including Aristide Maillol (1861-1944). She had acquired her collection of stained glasess, and in particular the pieces of the corpus here investigated, during the sale of the collection of Michel Acézay (1878-1944), himself a collector and painter-glassmaker working in Paris. He would have built his collection by going to meet his colleagues and convincing them to give them their pieces.

Supplementary Information B

Choice of the colorimetric system

We chose to calculate the colorimetric coordinates in the *Y xy* colorimetric system, rather than in the *L*a*b** colorimetric system. Two reasons lead to this choice: First, the *Y xy* system is less sensitive to the absorption background (due to the surface alteration of the glass) than the *L*a*b** system: the *x* and *y* coordinates are independent from a constant background. Second, the *Yxy* system allows plotting the colour on a two-dimensional plot, whereas the interpretation of *L*a*b** coordinates in terms of colour requires considering the three dimensions. In a *xy* plot, the lost third dimension (*Y*) is the total luminance, which does not alter the hue nor the saturation of the resulting colour, but its value (thus the brightness).

Light scattering at the surface of altered glasses increases the overall absorbance, hence *Y* values are underestimated. As scattering is isoenergetic, the shape of the spectrum is however preserved, so the *x* and *y* values for chromaticity are correctly evaluated. The conversion between *Yxy* and L*a*b* requires a good estimate of *Y*, thus L*a*b* results are not reliable in this case.

In the *Y xy* colorimetric system, three functions $\bar{x}, \bar{y}$ and $\bar{z}$ are defined. These three functions are the colorimetric functions of the standard observer CIE 1931. The shapes of the functions are given in Supplementary Fig. S7. The colorimetric coordinates *X*, *Y* and *Z* are then computed by projecting on each colorimetric function the product of the optical spectrum and the standard illuminant (here the D65 illuminant, average midday light in Western Europe). In this representation, the monochromatic (or fully saturated) colours lie on the horseshoe-shaped locus line (Fig. 1a), which accordingly describes the wavelengths of the full visible spectrum.

At the centre of this diagram is the white reference point. The distance of the experimentally measured colour to this white point defines the colour saturation.

$$\begin{cases} X = K \int_\lambda S(\lambda) I(\lambda) \overline{x}(\lambda) d\lambda \\ Y = K \int_\lambda S(\lambda) I(\lambda) \overline{y}(\lambda) d\lambda \\ Z = K \int_\lambda S(\lambda) I(\lambda) \overline{z}(\lambda) d\lambda \end{cases}$$

Where $S(\lambda)$ is the optical spectrum and $I(\lambda)$ is the power distribution of the illuminant. *K* is a normalisation factor, so that *Y* is the total brightness.

x, *y* and *z* are then obtained by normalising *X*, *Y* , *Z* so that $x+y+z = 1$.

$$\begin{cases} x = \frac{X}{X+Y+Z} \\ y = \frac{Y}{X+Y+Z} \\ z = \frac{Z}{X+Y+Z} \end{cases}$$

The calculations here presented were made by interpolating the CIE 1931 observer standards x, y, z and the D65 illuminant (average midday light in Western Europe) published by the CIE. Interpolation is needed because the observer standards have a 5 nm step size whereas the UV-visible spectrometer has 0.45 nm step size.

Supplementary Figure S1. (a) Left: Average thickness versus sample age; (b) Right: Thickness inhomogeneity (relative standard deviation) versus sample age.

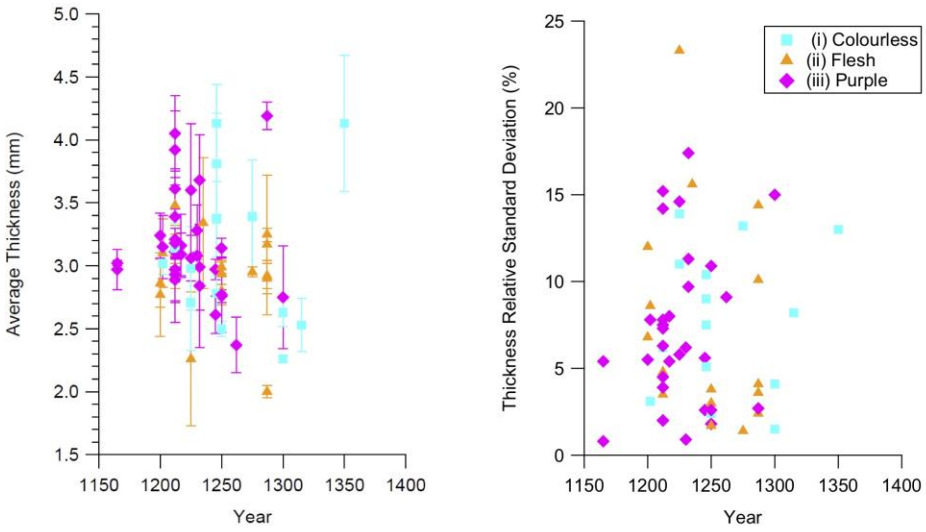

Supplementary Figure S2. Beer-Lambert trend lines of selected glasses after normalization at a 3mm thickness. They describe how colour changes with chromophore concentration.

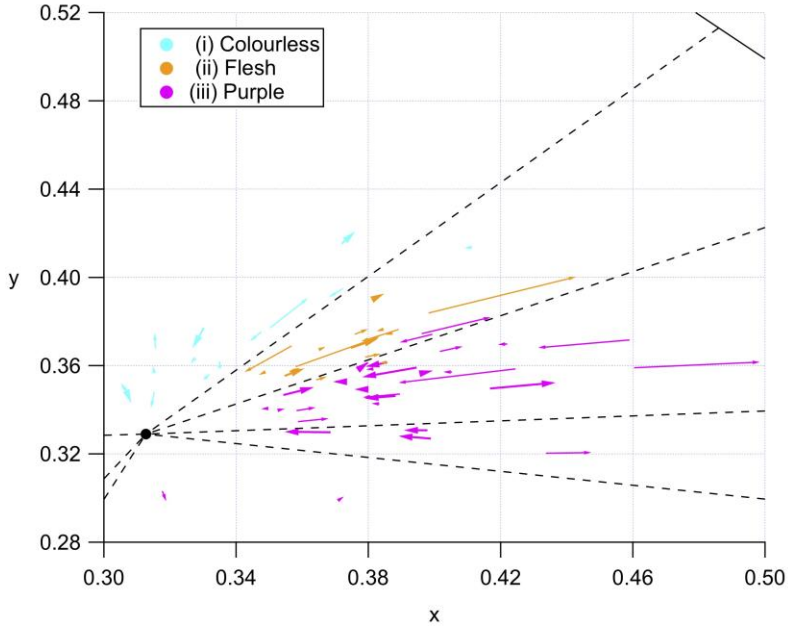

Supplementary Figure S3 a. Ternary plot of the chemical composition of the character heads: ternary plot of SiO_2 versus Na_2O+K_2O versus $CaO+MgO$.

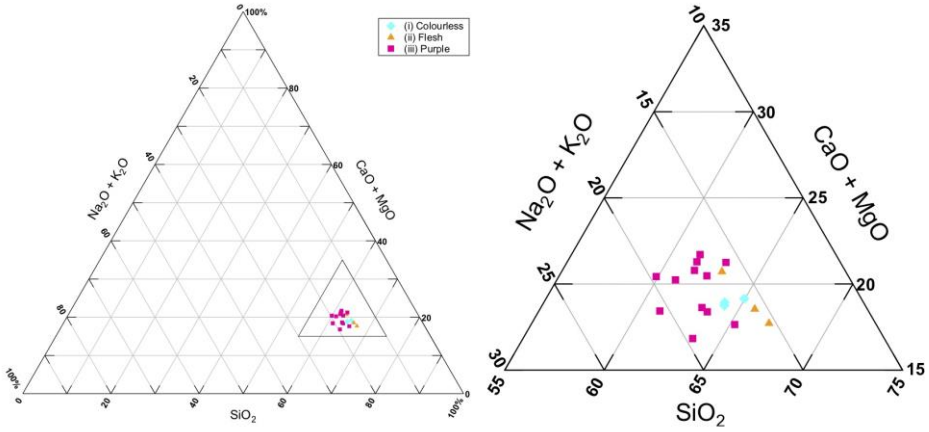

Supplementary Figure S3 b. Ternary plot of the chemical composition of the character heads: ternary plot of K_2O+MgO versus Na_2O versus CaO.

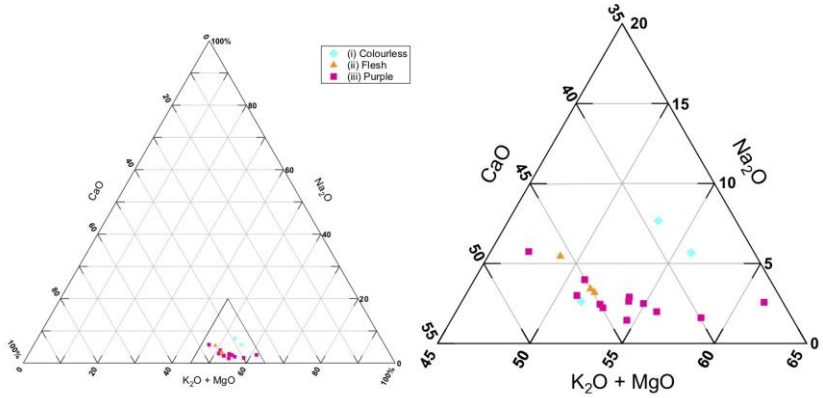

933 **Supplementary Figure S4.** Optical absorption spectrum of Mn^{3+} in a soda-lime glass, after the data of
934 Bamford (1977).
935

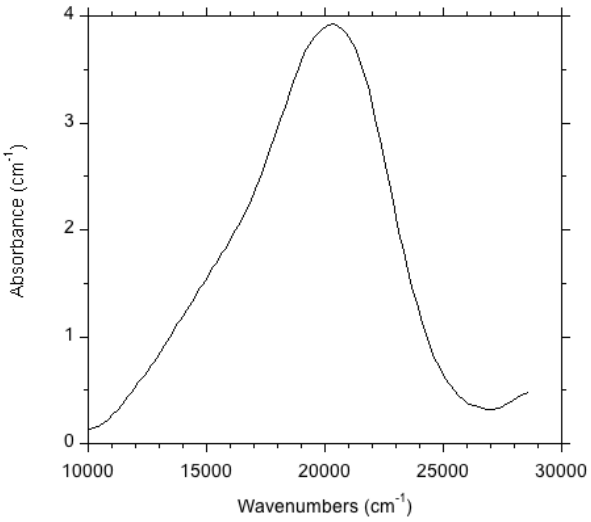

936
937

Supplementary Figure S5. Temporal variation of the colour of the stained glasses investigated. Colourless glasses are more recent than purple and flesh-tone glasses.

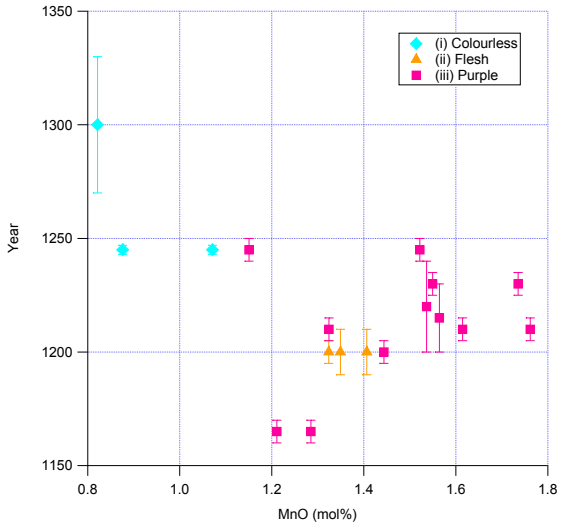

Supplementary Figure S6. Progressive reduction of Fe^{3+} introduced as Fe_2O_3 in a 28.2 Na_2O-71.8 SiO_2 sodium silicate melt at 1400°C. 100 g of melt with 0.4 wt.% were prepared in air in a Pt crucible. The solid curve is drawn through the data as a visual aid. After Calas and Miché, in prep.

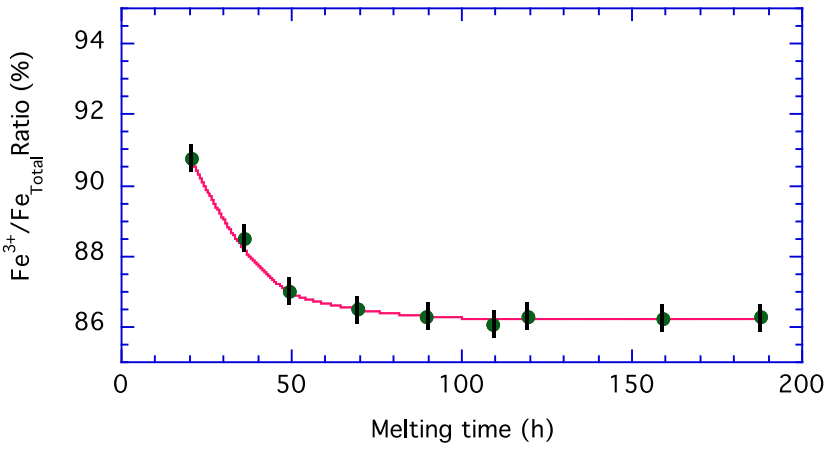

Supplementary Figure S7. Colorimetric functions of the standard observer CIE 1931

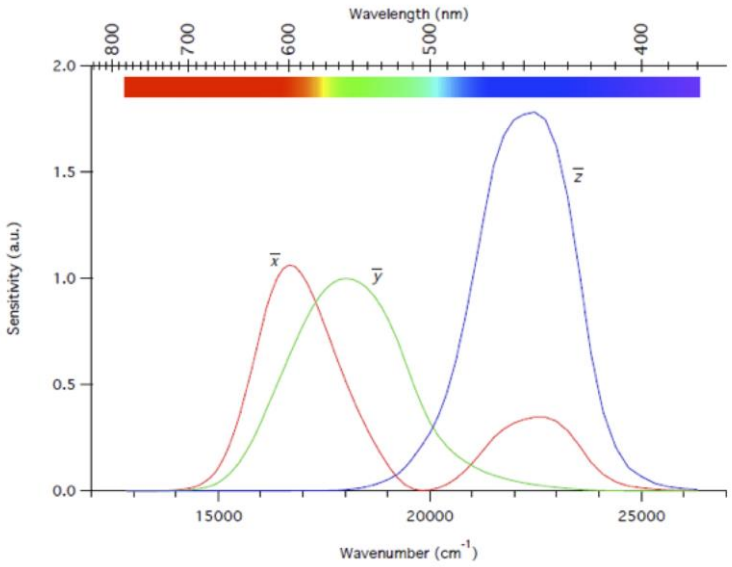

954 **Supplementary Table T1. Average thickness of the investigated samples.**

955

Glasses	Thickness
Purple	
41C*	3.02±0.02
41F*	2.97±0.02
42-3	3.28±0.20
43-1	4.05±0.30
43-2*	3.15±0.25
44-1	3.16±0.25
44-2	3.92±0.31
47-1	2.97±0.08
47-5F*	2.61±0.15
47-8	2.93±0.06
47-17*	2.99±0.34
47-25*	3.39±0.25
Flesh-tone	
42-2*	3.10±0.27
47-10*	2.86±0.19
47-23*	2.77±0.33
Colourless	
42-5*	3.81±0.40
44-3	4.13±0.31
47-28	2.53±0.21
Other (Yellow)	
47-5C	3.59±0.69

956

957

958

959 **Supplementary Table T2.** Colorimetric coordinates of the glasses of the whole Corpus, in Y*xy* and L*a*b*
960 systems, as calculated by the method described in 3.3, using the D65 illuminant.
961

Glasses	Y	*x*	*y*	L*	a*	b*
41C	0.82	0.398	0.331	7.38	8.16	3.13
41F	19.69	0.370	0.353	51.49	9.73	12.08
42-2	10.98	0.382	0.390	39.54	2.26	17.97
42-3	7.79	0.389	0.347	33.55	12.01	9.57
42-4	15.41	0.359	0.335	46.19	10.93	6.12
42-5	23.80	0.330	0.377	55.88	-8.39	13.11
42-6	0.52	0.384	0.376	4.71	1.51	3.38
42-7	16.68	0.350	0.377	47.85	-2.15	14.01
43-1	6.02	0.369	0.330	29.46	10.83	4.55
43-2	3.46	0.377	0.350	21.79	7.06	6.84
44-1	6.61	0.400	0.328	30.91	17.46	6.97
44-2	0.73	0.395	0.359	6.60	4.43	4.24
44-3	50.21	0.306	0.350	76.20	-10.78	5.28
44-4	16.75	0.315	0.348	47.95	-4.41	4.21
44-5	29.88	0.335	0.362	61.55	-2.91	11.12
44-6	5.32	0.461	0.360	27.62	19.65	17.27
47-1	7.10	0.380	0.362	32.03	7.03	10.82
47-2	0.30	0.379	0.364	2.74	1.13	1.66
47-3	5.66	0.389	0.377	28.53	5.43	13.07
47-4	5.73	0.356	0.357	28.73	3.10	7.46
47-5C	15.13	0.438	0.447	45.82	2.66	40.69
47-5F	39.13	0.354	0.347	68.84	8.91	11.03
47-6	2.07	0.364	0.354	15.84	3.72	5.42
47-7	1.64	0.396	0.357	13.49	6.76	7.15
47-8	22.55	0.366	0.368	54.60	4.66	15.51
47-9	25.61	0.375	0.368	57.67	7.32	17.48
47-10	0.36	0.318	0.303	3.29	1.45	-0.82
47-11	1.90	0.372	0.395	14.94	-0.38	9.83
47-12	0.56	0.406	0.358	5.03	4.18	3.40
47-13	30.78	0.330	0.354	62.32	-2.01	8.61
47-14	31.34	0.347	0.356	62.79	2.94	11.67
47-15	0.72	0.386	0.374	6.52	2.37	4.62
47-16	2.09	0.417	0.350	15.96	10.77	8.38
47-17	8.26	0.376	0.374	34.53	4.03	13.09
47-18	0.98	0.459	0.372	8.86	9.75	8.89
47-19	27.28	0.357	0.369	59.23	1.80	15.52
47-20	0.48	0.390	0.348	4.36	3.38	2.30
47-21	1.87	0.402	0.367	14.77	6.43	8.82
47-22	30.09	0.355	0.356	61.73	5.47	12.33
47-23	2.24	0.381	0.359	16.71	5.31	7.13
47-24	0.35	0.435	0.322	3.16	5.75	1.65

47-25C	0.52	0.386	0.362	4.70	2.47	2.91
47-25V	24.14	0.398	0.384	56.22	9.20	24.30
47-26	5.94	0.384	0.343	29.26	10.83	7.76
47-27	17.09	0.371	0.415	48.37	-5.48	24.51
47-28	11.23	0.430	0.494	39.97	-7.01	46.38
47-28Y	24.03	0.327	0.363	56.12	-5.38∑	9.55
47-29	4.79	0.425	0.359	26.13	13.76	13.03
47-30	1.13	0.372	0.301	10.05	10.36	0.01
47-32	42.88	0.347	0.375	71.47	-3.23	18.23
47-33	2.12	0.409	0.413	16.11	1.90	14.75
47-34	0.84	0.353	0.340	7.56	2.98	2.22
47-35	23.67	0.359	0.340	55.76	10.89	8.19
47-36	2.21	0.399	0.374	16.53	5.50	10.00
47-37M	1.03	0.358	0.360	9.24	1.69	4.36
47-37V	27.91	0.306	0.349	59.81	-8.50	4.11
47-38	41.28	0.315	0.357	70.37	-9.26	8.23
47-39	1.10	0.315	0.367	9.82	-3.74	3.30
47-40	8.78	0.422	0.370	35.55	13.90	17.65
47-41	0.87	0.396	0.375	7.86	3.72	5.94
47-42	17.64	0.370	0.382	49.06	1.67	17.72
47-44	15.27	0.385	0.362	46.00	10.23	14.62
47-45	3.68	0.351	0.341	22.57	4.57	3.97
47-46	15.27	0.385	0.362	46.00	10.23	14.62

The glasses analysed are not fully translucent, mostly because of light scattering due to the alteration of the glass surface. This slight opacity causes which results in overestimating the overall absorbance, hence *Y* values are underestimated. As scattering is isoenergetic, the shape of the spectrum is however preserved, so the *x* and *y* values for chromaticity are correctly evaluated.